

Discovery of potent and selective inhibitors of the *Escherichia coli* M1-aminopeptidase via multicomponent solid-phase synthesis of tetrazole-peptidomimetics

Yanira Méndez^{a,b,†}, German De Armas^{c,†}, Idalia Pérez^{c,‡}, Tamara Rojas^a, Mario E. Valdés-Tresanco^c, Maikel Izquierdo^c, Maday Alonso del Rivero^c, Yoanna María Álvarez-Ginarte^d, Pedro A. Valiente^{c,*}, Carmen Soto^c, Lena de León^c, Aldrin V. Vasco^b, William L. Scott^e, Bernhard Westermann^b, Jorge González-Bacero^{c,*} and Daniel G. Rivera^{a,b,*}

^aCenter for Natural Products Research, Faculty of Chemistry, University of Havana, Zapata y G, 10400, La Habana, Cuba

^bDepartment of Bioorganic Chemistry, Leibniz Institute of Plant Biochemistry, Weinberg 3, 06120, Halle/Saale, Germany

^cCenter for Protein Studies, Faculty of Biology, University of Havana, 25 y J, 10400, La Habana, Cuba

^dLaboratory of Theoretical and Computational Chemistry, Faculty of Chemistry, University of Havana, Zapata y G, 10400, La Habana, Cuba

^eDepartment of Chemistry and Chemical Biology, Indiana University Purdue University Indianapolis, Indianapolis, Indiana 46202, United States

[†]These authors contributed equally to this work.

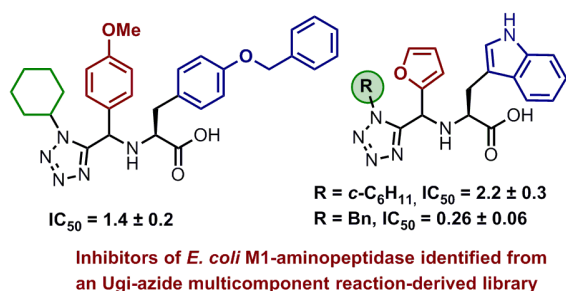
[‡]Permanent address: National Center for Biopreparation. Carretera de Beltrán km 1½, Bejucal, Mayabeque, 6048, Cuba

This is the author's manuscript of the article published in final edited form as:

Méndez, Y., De Armas, G., Pérez, I., Rojas, T., Valdés-Tresanco, M. E., Izquierdo, M., ... Rivera, D. G. (2018). Discovery of potent and selective inhibitors of the *Escherichia coli* M1-aminopeptidase via multicomponent solid-phase synthesis of tetrazole-peptidomimetics. *European Journal of Medicinal Chemistry*. <https://doi.org/10.1016/j.ejmech.2018.11.074>

*Corresponding authors. E-mail: jogoba@fbio.uh.cu (J. González-Bacerio), pedro.valiente79@gmail.com (P. Valiente), dgr@fq.uh.cu (D.G. Rivera)

Graphical Abstract



Abbreviations

AP, aminopeptidase; APN, neutral aminopeptidase; D3, Distributed Drug Discovery; ePepN, *Escherichia coli* neutral M1-aminopeptidase; 4CR, four-component reaction; I-MCR; isocyanide-based multicomponent reaction; Leu-*p*NA, L-leucine-*p*-nitroanilide; MAP, metallo-aminopeptidase; MD, Molecular Dynamics; PBC, periodic boundary conditions; pmAPN, porcine kidney cortex microsomes containing neutral aminopeptidase; SALI, Structure-Activity Landscape Index; SPS, solid phase synthesis; TPM, tetrazole-peptidomimetic.

Abstract

The *Escherichia coli* neutral M1-aminopeptidase (ePepN) is a novel target identified for the development of antimicrobials. Here we describe a solid-phase multicomponent approach which enabled the discovery of potent ePepN inhibitors. The on-resin protocol, developed in the frame of the Distributed Drug Discovery (D3) program, comprises the implementation of parallel Ugi-azide four-component reactions with resin-bound amino acids, thus leading to the rapid preparation of a focused library of tetrazole-peptidomimetics (TPMs) suitable for biological screening. By dose-response studies, three compounds were identified as potent and selective ePepN inhibitors, as little inhibitory effect was exhibited for the porcine ortholog aminopeptidase. The study allowed for the identification of the key structural features required for a high ePepN inhibitory activity. The most potent and selective inhibitor (TPM **11**) showed a non-competitive inhibition profile of ePepN. We predicted that both diastereomers of compound TPM **11** bind to a site distinct from that occupied by the substrate. Theoretical models suggested that TPM **11** has an alternative inhibition mechanism that doesn't involve Zn coordination. On the other hand, the activity landscape analysis provided a rationale for our findings. Of note, compound TMP **2** showed *in vitro* antibacterial activity against *Escherichia coli*. Furthermore, none of the three identified inhibitors is a potent haemolytic agent, and only two compounds showed moderate cytotoxic activity toward the murine myeloma P3X63Ag cells. These results point to promising compounds for the future development of rationally designed TPMs as antibacterial agents.

Keywords: multicomponent reaction, tetrazole, antibacterial, ePepN, molecular docking, protease inhibitor

1. Introduction

A cornerstone of infectious disease-based drug discovery is the identification of a single, but essential protein target that is prone to inhibition. This approach aims to boost the discovery of new targets besides those accounting for cell wall biosynthesis, membrane integrity, translation, transcription and DNA synthesis [1]. Proteases are final performers in the cytosolic degradation of proteins, an essential process in all living cells [2], and they participate in biologic processes as diverse as angiogenesis, antigen presentation or hormone processing. In addition, they are connected to pathologies such as hypertension, inflammation, while several studies describe their incidence in tumor-associated processes [3]. In bacteria, proteases are virulence factors targeting host proteins and tissues [4,5]. One of the most studied bacterial proteases is the neutral M1-alanyl aminopeptidase (AP) from the Gram negative bacterium *Escherichia coli* (ePepN) [2].

M1-APs are widely distributed throughout all phyla except for viruses, and comprise two conserved catalytic sequence motifs, *i.e.*, a consensus zinc-binding motif (HEXXH-(X₁₈)-E) and the 'GXMEN' exopeptidase motif [3]. ePepN, as all metallo-aminopeptidases (MAPs) belonging to this family, catalyzes the removal of polypeptide *N*-terminal amino acids throughout the nucleophilic attack of a water molecule that is activated by a Zn²⁺ cation [6–8]. Besides *E. coli*, human pathogens such as *Plasmodium falciparum*, the etiological agent of malaria, bear neutral APs (APNs) that are essential for their survival [9]. As a result, APNs are often considered therapeutic targets, and assessing their function, structure and inhibition is of significant interest for the scientific community [3].

ePepN has the highest ATP-independent AP activity in *E. coli*, and it participates in the last stages of the protein degradation pathway in the bacterium cytosol [5,10]. This enzyme carries out crucial functions in cellular maintenance, growth and development. The expression of the ePepN gene is increased in anaerobic conditions [11], as a response to the stress induced by chemical compounds, like sodium salicylate [5], and in minimal medium at high temperatures [12,13]. Despite not being essential in basal conditions [14], the AP activity of ePepN is required for a fast growth in the indicated circumstances [12,13].

Previously, we have described the utilization of isocyanide-based multicomponent reactions (I-MCRs) for the preparation of small combinatorial compound libraries targeting the M1-AP of *P. falciparum* [15] and *E. coli* [16]. Those reports comprised the solution-phase parallel synthesis of the library members by means of stepwise routes including the I-MCR and deprotection steps. In an endeavour to facilitate access to a focused library of potential AP inhibitors, herein we report the solid-phase multicomponent synthesis of novel tetrazole-peptidomimetics (TPMs) by the Ugi-azide four-component reaction (Ugi-azide-4CR) of resin-bound amino acids. We also report the evaluation of the inhibitory activity against ePepN for all library members, and the antibacterial activity of the most relevant compounds. Finally, similarity/activity cliffs analysis was performed in order to identify critical moieties for improving both the inhibitory and antimicrobial activities.

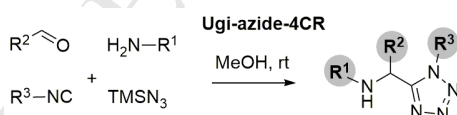
Compounds bearing the tetrazole ring have exhibited a wide range of medicinal applications, including analgesic, anti-inflammatory, antiviral and anticancer, among others [17]. Recent reports also highlight the antimicrobial activity of varied tetrazolic compounds against pathogenic bacteria and protozoa [18,19]. However, it was the metal-chelating

capacity of tetrazoles that caught our attention [20]. We hypothesized that suitably functionalized tetrazoles – i.e., armed with enzyme-active site matching functionalities – could inhibit the ePepN enzymatic activity via chelation of the Zn^{2+} cation.

2. Results and Discussion

2.1. Solid-phase multicomponent synthesis

To provide a fast and diversity-generating method for the assembly of TPMs, we sought to employ an I-MCR enabling the easy variation of the functionalities attached to the tetrazole ring. Thus, the Ugi-azide-4CR [21] was chosen because it provides an efficient access to 1,5-disubstituted tetrazoles [22] with three different sites of diversity generation, arising from the amine (R^1), carbonyl (R^2) and isocyanide (R^3) components (Scheme 1). Recently, several groups have extended the scope of the Ugi-azide-4CR to produce structurally diverse tetrazole-containing scaffolds [23–47], but relying on traditional solution-phase approaches.

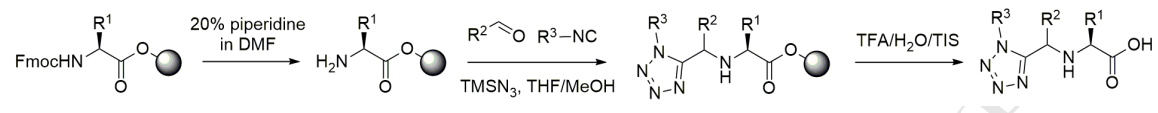


Scheme 1. The Ugi-azide-4CR using a protected amino acid as amino component.

We chose to implement a solid-phase protocol enabling the fast parallel synthesis of all library members and the subsequent evaluation of the ePepN inhibitory activity. Since the Ugi-azide-4CR has rarely been implemented on-resin [48-49], an initial assessment of the synthetic efficiency of the solid-phase procedure was done prior to the construction of the combinatorial library for biological screening. Thus, among all solvent mixtures tested for

the on-resin Ugi-azide-4CR, the best one turned out to be THF/MeOH 1:1 (v/v), which guaranteed the solubility of all reactants and led to full conversion in 72 h.

Table 1. Solid-phase synthesis of tetrazole-peptidomimetics by on-resin Ugi-azide-4CR.



Compound ^a	Amino acid (R ¹)	R ²	R ³	Yield (%) ^b	d.r. ^c
1	Tyr(Bzl)	H	cyclohexyl	60	-
2	Tyr(Bzl)	<i>p</i> -OMe-phenyl	cyclohexyl	83	2:1
3	Trp	H	cyclohexyl	65	-
4	Trp	2-furyl	cyclohexyl	73	1:1
5	Trp	<i>p</i> -OMe-phenyl	cyclohexyl	83	1.4:1
6	Trp	2-imidazolyl	cyclohexyl	60	1:1
7	Trp	3-pyridyl	cyclohexyl	81	1.7:1
8	Val	<i>p</i> -OMe-phenyl	cyclohexyl	80	3:1
9	Val	2-imidazolyl	cyclohexyl	68	2:1
10	Val	3-pyridyl	cyclohexyl	68	3:1
11	Trp	2-furyl	benzyl	83	1.4:1
12	Trp	<i>p</i> -OMe-phenyl	benzyl	80	1.4:1
13	Trp	2-imidazolyl	benzyl	69	1.6:1
14	Val	H	benzyl	61	-
15	Val	2-imidazolyl	benzyl	64	1.6:1
16	Val	<i>p</i> -OMe-phenyl	benzyl	73	3:1
17	Val	H	3-phenyl-propyl	63	-
18	Val	<i>p</i> -OMe-phenyl	3-phenyl-propyl	85	3.4:1
19	Val	2-imidazolyl	3-phenyl-propyl	60	4.7:1
20	Phe	2-furyl	cyclohexyl	66	1:1
21	Phe	2-furyl	benzyl	75	1:1

^aAll compounds were purified to >95% HPLC purity. ^bYield of pure isolated products. ^cDetermined by ¹H NMR

Following the concept of the D3 program [50,51], which focuses on simple, powerful and reproducible approaches for drug discovery, the parallel on-resin Ugi-azide-4CRs were implemented with resin-bound amino acids using the D3 Bill-Board-6-pack apparatus. As

shown in Table 1, amino acids having hydrophobic side chains, such as Phe, benzyl-protected Tyr, Trp and Val, were chosen to assemble TPM scaffolds, aiming at favouring the hydrophobic interactions within the enzyme active site. Of note, Phe, Trp and Tyr have been previously described as ePepN inhibitors [52] – a fact that supports the decision of using them for the multicomponent derivatization. The overall solid-phase protocol comprises the deprotection of the resin-bound (Wang resin, loading 1-1.5 mg/mmol) amino acids by Fmoc removal, followed by the on-resin Ugi-azide-4CRs for 72 h and final cleavage from the resin. A simple purification procedure using cyanosilica cartridges rendered the final compounds in good overall yield and purity suitable for biological evaluation (*i.e.*, >95 % as determined by HPLC). A variety of available carbonyl and isocyanide components were employed in the parallel syntheses, producing a total of 21 new TPMs. In most cases, the choice was to introduce hydrophobic substituents at R² and R³, some of them even bearing metal chelating moieties like the pyridyl. The aldehyde components enabled the incorporation of substituents such as 2-furyl, *p*-OMe-Ph, 3-pyridyl and 2-imidazolyl. Due to the poor stereoselectivity of the Ugi-azide-4CR, the use of these latter aldehydes rendered the final products as a mixture of two diastereomers, which could not be separated by column chromatography. As a result, such compounds were subjected to biological evaluation as a mixture of diastereomers. In order to assess the effect of such substituents, we also chose to prepare compounds derived from formaldehyde as carbonyl component, for which we relied on an aminocatalysis-mediated transimination protocol recently developed by our group [53–55]. Thus, the on-resin Ugi-azide-4CR reaction with paraformaldehyde consisted of imine formation by transimination of the resin-bound amino acid in THF/MeOH 1:1 (*v/v*) – using the piperidinium ion derived from previous reaction of

paraformaldehyde and piperidine – followed by addition of the isocyanide component and TMSN_3 and shaking for 72 h.

2.2. Biological evaluation

2.2.1. Evaluation of the TPMs as ePepN inhibitors

In order to evaluate the inhibition of the recombinant ePepN enzyme by the tetrazole-peptidomimetics, dose-response studies were performed and the IC_{50} values were determined. A dose-dependent reversible inhibition was obtained for all the inhibitors (see curves in Fig. S1, Supplementary Material) using a pre-incubation step of 15 min to reach the equilibrium. The IC_{50} values vary from 0.26 μM to more than 1000 μM (Table 2). Thus, seven TPMs showed IC_{50} values higher than 100 μM (*i.e.*, **3**, **5**, **9**, **16**, **17**, **18** and **19**), ten TPMs showed IC_{50} values in the range 10-100 μM (*i.e.*, **1**, **6**, **7**, **8**, **10**, **13**, **14**, **15**, **20** and **21**), three TPMs between 1 and 10 μM (**2**, **4** and **12**), and one lower than 1 μM (**11**).

Table 2. Inhibition of recombinant ePepN by the Ugi-azide-4CR derived TPMs.

Compound	Structure	IC_{50} (μM) ^a	Compound	Structure	IC_{50} (μM) ^a
1		44 ± 5	2		1.4 ± 0.2
3		110 ± 4	4		2.2 ± 0.3
5		630 ± 50	6		48 ± 4

7		22 ± 2	8		90 ± 4
9		127 ± 2	10		27 ± 2
11		0.26 ± 0.06	12		7.2 ± 0.9
13		25 ± 1	14		47 ± 4
15		71 ± 3	16		> 1000
17		170 ± 10	18		160 ± 10
19		470 ± 20	20		41 ± 3
21		17.0 ± 0.9	bestatin		7 ± 4

^aThe data are presented as the mean ± the standard error.

These results allow for conducting a preliminary structure-activity relationship analysis for the TPM combinatorial library. For example, the comparison of TPMs **1** and **2**, both derived from Tyr(Bzl) and cyclohexyl isocyanide, suggests that the presence of the central *p*-OMe-phenyl group at R² favours the ePepN inhibition, compared with the lack of substituent in this position (Table 2). In this sense, compound **2** can be considered as a potent inhibitor of the target enzyme, showing an IC₅₀ value of 1.4 μM.

In the series of the five TPMs bearing the cyclohexyl and indole moieties (*i.e.*, **3**, **4**, **5**, **6** and **7** derived from Trp), both the lack of R² substituent and the presence of *p*-OMe-phenyl at this position proved unfavourable for the inhibition of ePepN. Alternatively, the greatest potencies in the inhibitory activity were obtained for TPMs with the substituents 2-furyl, 2-imidazolyl and 3-pyridyl at position R². Thus, TPM **4** bearing the 2-furyl moiety proved to be the most active one of this series.

Interesting results were also obtained for the series of TPMs derived from benzyl isocyanide (*i.e.*, R³ = Bn). For example, the combination of benzyl at R³ and Trp as amino acid resulted in the active compounds **11** (R² = 2-furyl) and **12** (R² = *p*-MeO-phenyl), **11** being the most potent inhibitor among all tested compounds. In contrast, the amino acids Val and Phe did not afford very active compounds in any of the combinations of aldehyde and isocyanide components. The lack of a central substituent at R² or the presence of the imidazole group in this position resulted in compounds with poor inhibitory activity against ePepN. As a partial summary of this analysis, we may conclude that amino acids in position R¹ with bulky aromatic side chains like those of Trp and benzyl-protected Tyr, provide very active TPMs when combined in position R³ with either aliphatic (cyclohexyl) or aromatic (Bn) isocyanides and an aromatic aldehyde. Thus, to obtain good ePepN inhibitors, this class of TPM skeleton requires an aromatic side chain at R¹ position, while the R³ substituent can be either aliphatic or aromatic, but it must be a bulky substituent enabling favourable hydrophobic interactions with the enzyme binding site. As the three compounds showing the best inhibitory activity against ePepN were evaluated as diastereomeric mixtures, we tried the separation of each stereoisomer by semi-preparative RP-HPLC. Unfortunately, after various attempts with different solvent systems, it was not possible the

resolution of two peaks for compounds **2**, **4** and **11**, using a standard C-18 column (see analytical HPLC traces in the Supplementary Material). This was unfortunate, because some of the non-active compounds appear as two separate peaks in RP-HPLC and could have been separated in case of good inhibitory activity.

The inhibition of the recombinant ePepN enzyme by TPMs incorporating such hydrophobic substituents is coherent with other literature reports. For example, the favourable hydrophobic interactions between the bestatin's benzyl group and the APNs' active site have been well described [2,56–58]. Other examples come from the work of Addlagatta *et al.* [52], who verified by X-ray crystallography of ePepN–amino acids complexes that the enzyme's active site can accommodate well the side-chains of phenylalanine, tyrosine and tryptophan.

2.2.2. Assessment of the selectivity in the inhibition of bacterial versus mammalian APNs

As a result of the dose-response studies, the TPMs **2**, **4** and **11** were selected for further biological studies regarding the selectivity for the APNs. We performed dose-response studies with these compounds toward porcine kidney cortex microsomes containing neutral aminopeptidase (pmAPN), using the L-leucine-*p*-nitroanilide (Leu-*p*NA) substrate (Table 3 and Fig. S2). In this manner, it was observed that the three inhibitors are highly selective for ePepN with selectivity indexes higher than 900, as compared with its porcine ortholog APN in the context of the microsomal fraction. This selectivity can be considered as a very relevant result, as it is an essential requirement for the potential therapeutic use of these compounds, and such selectivity indexes are not frequent in many AP inhibitors reported so far. For example, in addition to the general inhibitor of the M1- and M17-APs, *i.e.*, bestatin,

very few micromolar or submicromolar inhibitors of ePepN have been reported [59,60]. It is important to explain that the inhibition potency towards ePepN is expressed with the IC_{50} parameter, and not with the inhibition constant (K_i), since the recombinant ePepN was not purified to reach the total homogeneity (>90 % of purity), as it was not pmAPN.

The use of microsomes from porcine kidney cortex, instead of purified porcine APN, for the enzymatic inhibition assays, is based on the work of Byzia *et al.* [61]. These authors demonstrated that the kinetic properties of soluble porcine APN are very similar to those showed by the membrane-associated enzyme. For this reason, the extraction and purification of the protein is not necessary for the screening of inhibitors. As a negative aspect of this methodology, it should be taken into account that a fraction of the inhibitor could be either distributed in the lipid bilayer on this heterogeneous system or interact with the acid AP, another M1-family member of MAPs which is co-localized with the APN in the kidney cortex membrane [62]. In both cases, the inhibitory potency toward the porcine enzyme would be underestimated, and the selectivity for ePepN would be overestimated. However, the use of the microsomal fraction in the assays allows reproducing better the microenvironment in which an inhibitor would act in a future therapeutic application, where it would face the APN bound to the plasmatic membrane in different cellular types and tissues [63].

Although the architecture of the APNs' active sites is well conserved among different species, there are structural variations that determine the differences in the affinity by distinct ligands. For example, Met²⁶⁰ of ePepN is substituted by Ala in the porcine and human APN, which leads to variations in substrate specificity and kinetic parameters [64].

These differences between the active sites of ePepN and mammalian APN could be responsible for the inhibition selectivity of compounds **2**, **4** and **11**.

Table 3. Dose-response studies for the inhibition of the pmAPN aminopeptidase by the three most potent TPM inhibitors of the ePepN enzyme.

Compound	IC ₅₀ pmAPN (μM) ^a	IC ₅₀ rePepN (μM) ^a	Selectivity index (IC ₅₀ (pmAPN)/IC ₅₀ (rePepN))
2	1,580 \pm 20	1.4 \pm 0.2	1,128
4	2,000 \pm 500	2.2 \pm 0.3	909
11	6,100 \pm 700	0.26 \pm 0.06	23,461

^aThe data are presented as the mean \pm the standard error.

2.2.3. Partial kinetic characterization of selected ePepN inhibitors

For compound **11**, the most potent and selective toward the recombinant ePepN enzyme, it was observed that a 15-min pre-incubation time for the ePepN/inhibitor mixture is enough to reach the inhibition equilibrium (Fig. 1A). In addition, it was determined that **11** is a non-competitive inhibitor ($\alpha < 1$) of this *E. coli* AP (Fig. 1B).

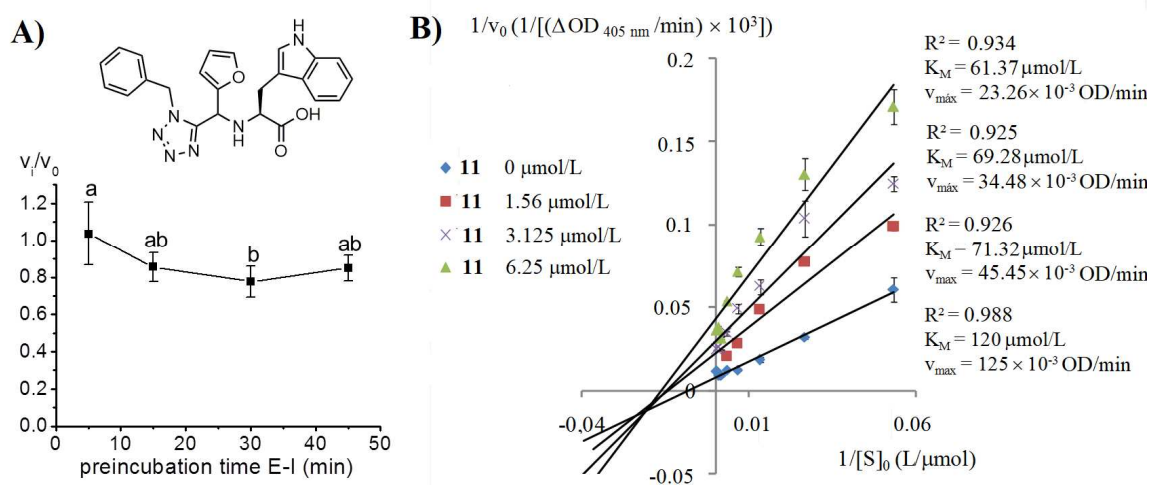


Figure 1. Kinetic characteristics for the inhibition of ePepN by compound **11**. A) Study of the enzyme/inhibitor pre-incubation time necessary to reach the inhibition equilibrium. E: enzyme. I: inhibitor. Different letters represent significant differences for $p < 0.05$. B) Determination of the

inhibition type. The K_M and v_{max} values are apparent. All data are presented as the mean \pm the standard deviation.

The fact that TPM **11** is not a competitive inhibitor of the *E. coli* enzyme suggests that the identified ePepN inhibitors could bind the enzyme at a region different to that of the active site, although maintaining some influence on the conformation of this cavity. The knowledge of the kinetic type of inhibition of a target enzyme by a family of structurally-related compounds is of vital importance both to elucidate the inhibition mechanism and to guide the optimization of the molecule's scaffold seeking for a higher potency and selectivity. Besides, it facilitates the *in silico* studies for the binding mode of the inhibitor to the enzyme and contributes to the design of new inhibitors. In the case of ePepN, there is no literature evidence regarding kinetic studies aimed at assessing the type of inhibition mechanism of this enzyme. Therefore, the determination in this work that the mode of ePepN inhibition – by **11** – is non-competitive ($\alpha < 1$) represents a relevant contribution to this field.

2.2.4. Computational studies of the putative binding modes of the ePepN–TPM **11** complexes

In order to investigate the binding modes of the most active TPMs to ePepN, structural analysis, molecular docking, MD simulations and free energy calculations were combined. For this, we took advantage of the available experimental data to support the docking process (receptor selection, search space definition) and selection of the final models. MD simulations and binding free energy calculations using the LIE method [65] were employed for assessing the stability of the predicted poses for each complex.

First, the focus was on searching for a proper receptor for docking simulations, because many structures of ePepN enzyme are available at PDB. The analysis of 37 ePepN structures retrieved from PDB showed coincident positions for almost all residues at the active site. However, Met²⁶⁰, which is involved in substrate recognition, showed a high degree of conformational diversity among all analysed structures (see Fig. S3). It has been described that the conformation of this residue in the ligand-free form of the enzyme differs from that of the ligand-bound [2,52,66]. Therefore, the conformation of this residue in the selected receptor was crucial to ensure the quality of the final models. Additionally, other residues far away from S1 site showed a high flexibility (see Fig. S3). Finally, before selecting the receptor, not only the structural analysis was considered, but also the kinetic characterization of the most active compound, *i.e.*, **11**.

Taking into account both the structural and experimental data, we chose as target the 3D structure of ePepN (PDB ID: 4XNB) in complex with L- β -homophenylalanine (L- β -HPheAla), a substrate-like inhibitor. In this structure, the side chain of Met²⁶⁰ swings out from the S1 hydrophobic pocket, providing space for the phenyl side chain of L- β -HPheAla. L- β -HPheAla was removed from the active site of the enzyme before starting docking simulations.

Similar binding modes were predicted for both TPM **11** isomers, although with different scores. TPM **11_S** exhibited a score of -10.1 kcal/mol, while the score for TPM **11_R** was -7.8 kcal/mol. According to our models, the Met²⁶⁰ side chain served as anchoring point to the central core of the inhibitors (Fig. 2). In both cases, the R³ moiety linked to the tetrazole ring interacted with the residues Met²⁶⁰, Asn³⁷³, Asn³⁷⁴, Tyr³⁷⁶, Gln⁸²¹, Ser⁸²⁴ and Arg⁸²⁵, located in a pocket with a volume similar to that of benzyl group. It is worth noting that this

pocket becomes accessible when the substrate binds, and that both Met²⁶⁰ and Arg⁸²⁵ approach to each other and interact through hydrogen bond (Fig. S4).

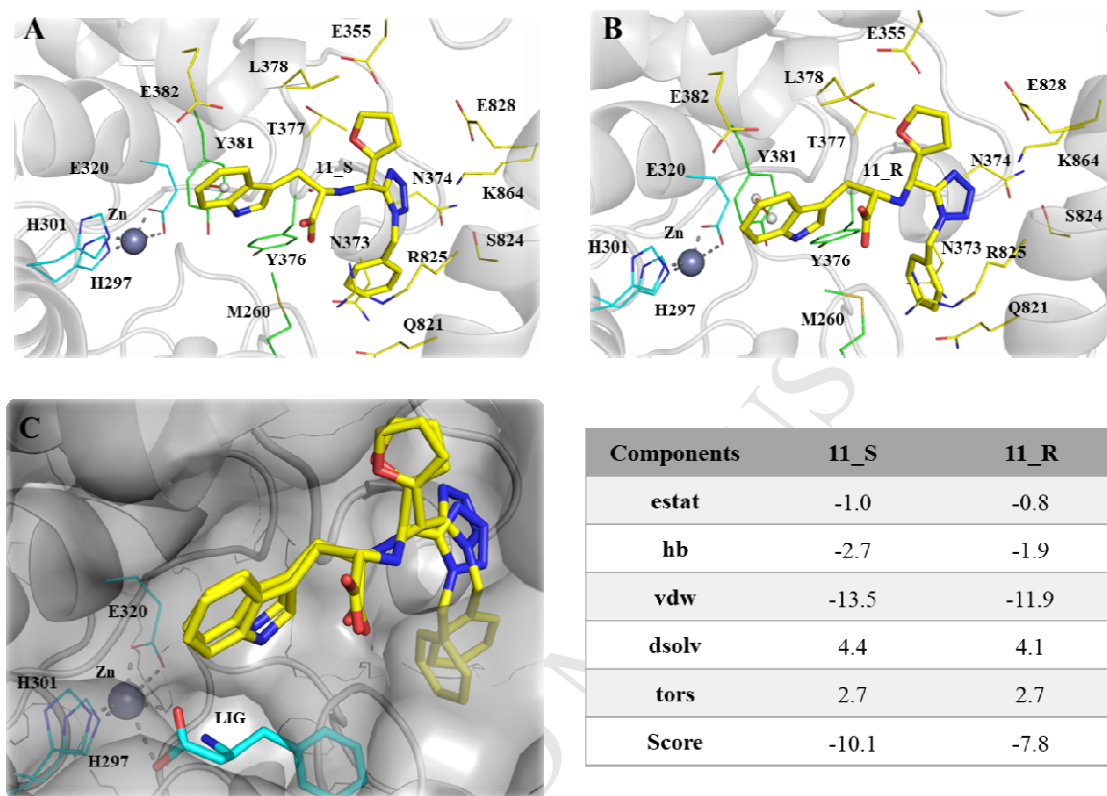


Figure 2. Binding mode of the ePepN:TPM **11** complexes A) ePepN:TPM **11_S**, B) ePepN:TPM **11_R**. Both diastereomers are represented as stick. Color codes: inhibitor atoms: carbon in yellow, oxygen in red, and nitrogen in blue. Residues belonging to substrate binding site are represented as lines and colored as follows: carbon in green, oxygen in red, and nitrogen in blue. The Zn atom is represented as a grey sphere. The π - π -stacking and Zn coordination bonds are represented orange and grey dotted lines, respectively. For clarity, we don't represent the hydrogen bonds and the van der Waals interactions. C) Superposition of the modelled complexes in a surface diagram of ePepN active site. Substrate-like inhibitor L- β -HPheAla is depicted as sticks. Color codes: L- β -HPheAla atoms: carbon in cyan, oxygen in red, and nitrogen in blue. Table in right shows the energetic components (in kcal/mol) as depicted in AD4 scoring function: estat (electrostatic), hb (hydrogen bond), vdw (van der Waals), dsolv (desolvation) and tors (torsional).

On the other hand, the indole-methyl group in both isomers interacted through π - π -stacking with Tyr³⁸¹, a residue involved in the stabilization of the tetrahedral transition state. Intriguingly, the TPM did not coordinate the zinc ion in the active site (Fig. 2). It was also observed a prevalence of hydrophobic interactions with aliphatic (Leu³⁷⁸), polar (Thr³⁷⁷), aromatic (Tyr³⁷⁶) and charged (Glu³⁵⁵, Glu³⁸², Glu⁸²⁸, Arg⁸³², and Lys⁸⁶⁴) residues (Fig. 2). The critical differences in the predicted binding mode for both diastereomers are the accommodation of the benzyl group as well as, the formation of a hydrogen bond between TPM **11_S** and the carbonyl group of Tyr³⁷⁶. The former cannot be established with TPM **11_R** since the N-H group is in the opposite direction to that of TPM **11_S** (Fig. 2). The absent of this hydrogen bond in the predicted binding mode for TPM **11_R**, accounts for a score decrease in ~ 1.0 kcal/mol.

To understand the non-competitive inhibition profile, it was critical to address the inhibitor interactions with residues enrolled in the substrate binding pocket and other putative subsites. For comparison purposes, we aligned the 3D structure of the ePepN:L- β -HPheAla complex over the predicted ePepN:inhibitor complexes to generate ternary ePepN:L- β -HPheAla:inhibitor complexes (Fig. 2C). As expected for non-competitive inhibitors, none of the isomers interacted with most residues belonging to the substrate binding site, leaving unoccupied spaces that allow inhibitor and substrate binding to the enzyme at the same time (Fig. 2C). Furthermore, interaction with Tyr³⁸¹, a critical residue for catalysis, supported the non-competitive inhibition mode. These results are similar to those described for compounds BTB11079, JFD00064, and BTB07018, all non-competitive inhibitors of mammalian APNs [67].

The predicted complexes were subjected to MD simulations in order to assess the stability of the predicted binding modes. The inspection of the trajectories and free energy profiles revealed that complexes of both diastereomers remained stable during the whole MD simulations (30 ns) (Fig. 3). Throughout MD simulations, we observed a similar interaction pattern as compared with that predicted by docking. Both diastereomers fit well into the active site, by interacting with a common group of aminoacids (Met²⁶⁰, Leu³⁵¹, Asn³⁷³, Asn³⁷⁴, Tyr³⁷⁶, Thr³⁷⁷, Leu³⁷⁸, Tyr³⁸¹, Glu³⁸², Gln⁸²¹, Ser⁸²⁴, Arg⁸²⁵, Glu⁸²⁸, and Lys⁸⁶⁴) (Fig. 3). Nevertheless, and as expected, slight differences were observed, because of a more accurate description of the interactions, explicit consideration of solvent effects and complexes dynamic itself. Called our attention the interaction of diastereomer **11_S** with His²⁹⁷, a residue coordinating the Zn²⁺ ion. By interacting simultaneously with both, His²⁹⁷ and the catalytic Tyr³⁸¹, the indole-methyl group was placed at the S1 site entrance.

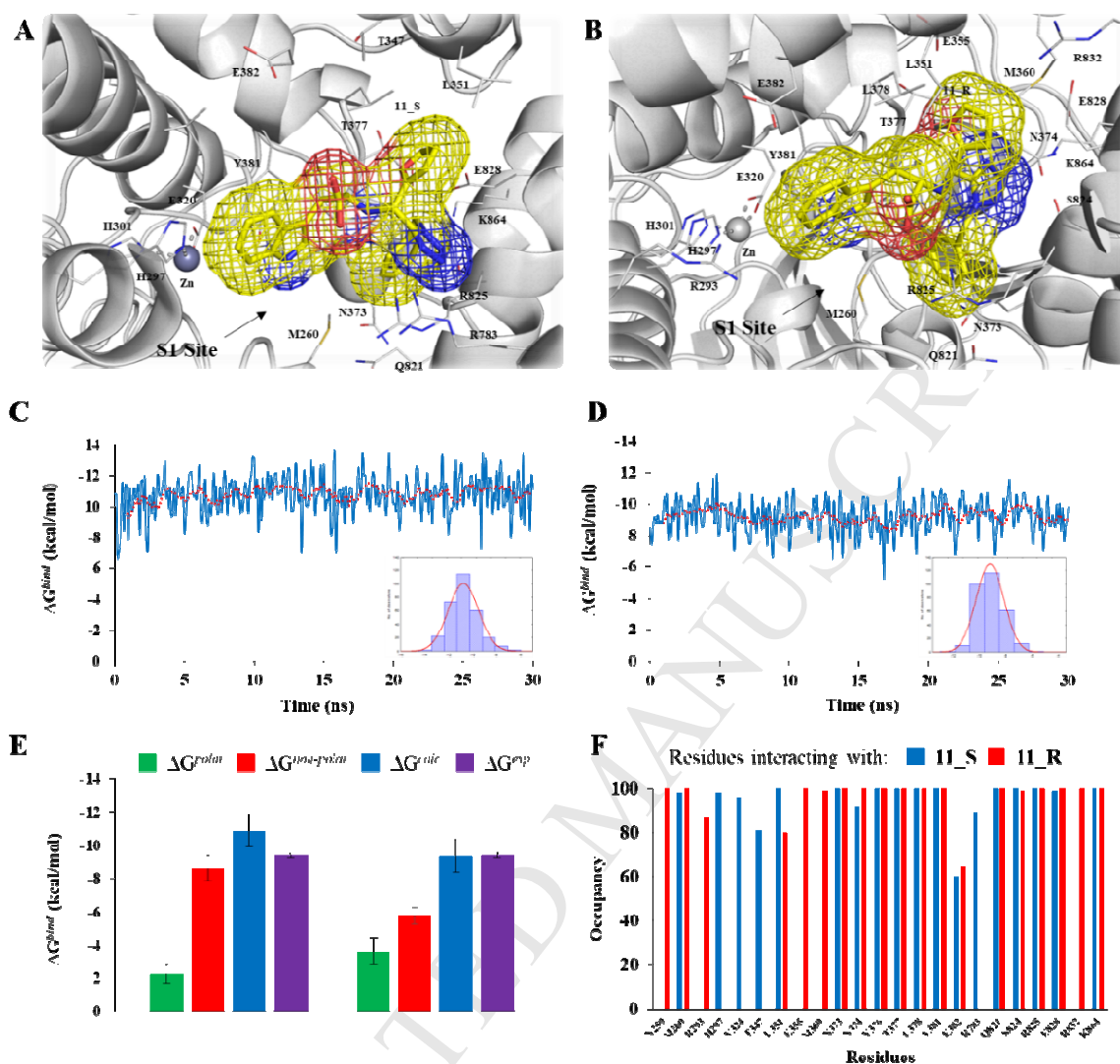


Figure 3. Results from MD simulations for ePepN:TPM 11 complexes. Final structures of A) ePepN:TPM 11_S, B) ePepN:TPM 11_R, after 30 ns. Both diastereomers are represented as stick. Also, the inhibitors have been rendered as mesh, to give an impression of overall volume. Colour codes: inhibitor atoms: carbon in yellow, oxygen in red, and nitrogen in blue. Free energy profiles for predicted complexes C) ePepN:TPM 11_S and D) ePepN:TPM 11_R. Histograms showing normal distribution of calculated binding free energies, are included. E) Contributions to binding free energy of each ePepN-inhibitor complex (left 11_S, right 11_R) using LIE-D method. Green bars represents the statistical values (mean \pm standard deviation) for polar contribution (ΔG^{polar}), red bars represents the statistical values (mean \pm standard deviation) for non-polar contribution ($\Delta G^{non-polar}$) to binding, blue bars represents the statistical values (mean \pm standard deviation) for calculated binding free energies (ΔG^{calc}), and purple bars represents the statistical values (mean \pm standard

deviation) for experimental binding free energy (ΔG^{exp}). F) Average occupancy percentage of all the residues located at less than 4.0Å from the inhibitors. For clarity, only those residues with an average occupancy above 50 % are showed.

Free energy calculations with the LIE-D method supported docking predictions. Again, from binding free energy calculations it was possible to predict that the complex **11_S**-ePepN ($\Delta G^{bind} = -10.9$ kcal/mol) was more stable than the complex **11_R**-ePepN ($\Delta G^{bind} = -9.4$ kcal/mol). Our results showed that both, the non-polar ($\Delta G^{non-polar} = \alpha \Delta \langle V_{i-s}^{vdW} \rangle + \gamma$) and polar ($\Delta G^{polar} = \beta \Delta \langle V_{i-s}^{el} \rangle$) contributions, were favourable for the binding of both diastereomers (Fig. 3).

To sum up, by combining molecular docking, MD simulations and free energy calculations we explained the non-competitive ($\alpha < 1$) profile observed for TPM **11** in the kinetic assays. We observed that both diastereomers bound in a different site to that of the substrate and interacting with Tyr³⁸¹, a critical residue for catalysis. In addition, they filled a pocket located near from S1 site (Fig. 3). This pocket is created when the substrate binds and Met²⁶⁰ side chain moves away from S1 site (Fig. S4). That way, the substrate must bind first before the inhibitor does. We believe that the inhibition could proceed mostly by interacting with catalytic Tyr³⁸¹ or blocking sterically product exit from the active site. Both variants are perfectly possible because of the presence of bulky hydrophobic substituents able to interact either with Tyr³⁸¹ or trapping the product into the active site.

2.2.5. Activity landscape modelling

Activity landscape modelling, allowed us to explain the observed structure-activity relationships. Similarity analysis based on *FragFp* descriptor [68], showed two main clusters with almost the same number of compounds, but a remarkable difference in activity

(Fig. 4). Cluster number 1 containing nine compounds (*i.e.* **8**, **9**, **10**, **14**, **15**, **16**, **17**, **18**, and **19**) showed an average pIC₅₀ of 3.88. All these inhibitors contain an isopropyl function at R¹ (Fig. S5). According to the proposed models (Fig. 2 and 3), isopropyl function is unable to establish optimal interactions with Tyr³⁸¹ at the active site, which may justify the low activity of these compounds. On the other hand, cluster number 2 with eight compounds (*i.e.* **3**, **4**, **5**, **6**, **7**, **11**, **12**, and **13**), showed an average pIC₅₀ of 4.64. Conversely, all the inhibitors contain the indole-methyl function at R¹, which is able to establish optimal π - π -stacking interactions with Tyr³⁸¹ at the active site, thus justifying the higher activity of these compounds (Fig. 2, 3 and S5). TPMs **20** and **21**, having intermediate properties, showed up between the two main clusters. TPM **2** was related mostly to TPMs **5** and **8**. Finally, TPM **1** was related only to TPM **2**.

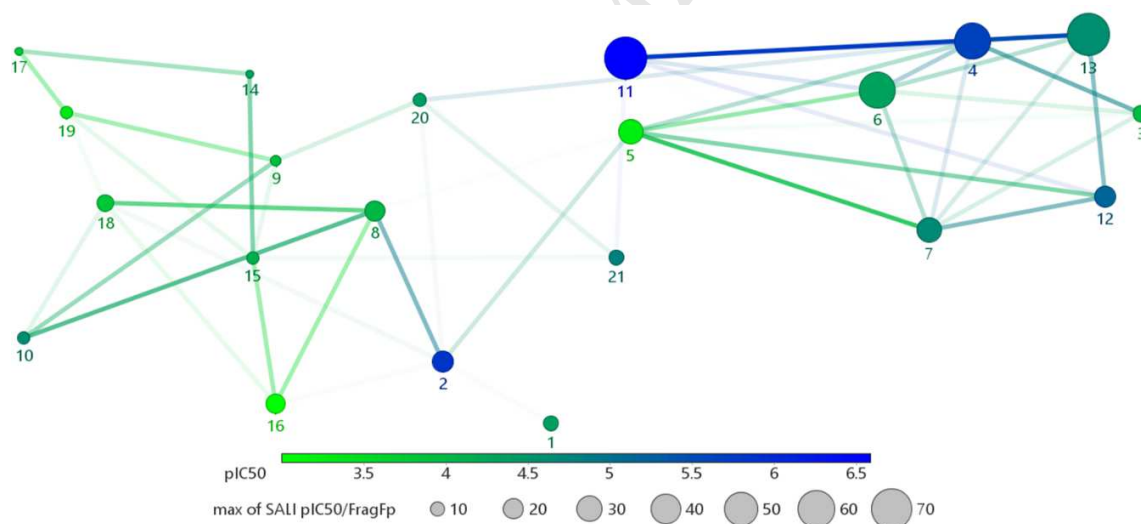


Figure 4. SALI 2D-Plot of studied series. Compounds are shown as spheres in 2D space. Size and colour of the sphere represent maximum values of SALI for each compound and pIC₅₀, respectively. Lines connect compounds with a similarity index above 85 % (neighbours). Code of the compound is shown below the corresponding sphere.

The highest SALI values were observed for TPMs **11** and **13**, both with SALI = 78. The only difference between these compounds is related to the central function. TPM **11** has a 2-furyl function, while TPM **13** has an imidazole. Thus, exchanging these chemical functions with each other causes a dramatical effect on the activity. An identical effect was observed for TPMs **4** and **6** (SALI = 56) with 2-furyl and imidazole functions, respectively. In the case of imidazole, the unfavourable interactions established with the enzyme's active site could be due to not to the volume but the electronic distribution.

The analysis of activity landscape, has become a popular method for characterizing structure-activity relationships [69,70]. Activity landscape modelling crucially depends on molecular representations and similarity metrics used to assess structural similarity [69]. Here, the structural similarity analysis was based on the *FragFp* descriptor. The *FragFp* descriptor is based on a predefined dictionary of 2D structural fragments. This is recommended because it does not require 3D information and similarity calculations are practically instantaneous [71]. Similarity threshold was set to 85 %, in order to get a well equilibrated distribution in terms of similarity relationships and number of clusters. Beyond mere visualization, we employed SALI values for quantitatively characterizing activity landscape features. Originally, SALI scores have been utilized to identify activity cliffs as compound pairs [72].

The analysis of the other functions at R² and R³, allowed explaining not only the variability in the observed activity between clusters, but also inside of each cluster. In general, having 2-furyl and benzyl functions at R² and R³, favours the inhibitory activity. Conversely, having voluminous *p*-methoxy-phenyl and 3-phenyl-propyl functions at R² and R³, is unfavourable (Fig. S5). A pleasant surprise came with TPM **2**, since it was identified as a

potent inhibitor of ePepN, even when having a voluminous *p*-methoxy-phenyl group at R². TPM **2** is related to TPMs **5** and **8**, both having a *p*-methoxy-phenyl group at R², but with a poor inhibitory activity. Notably, the only difference between these compounds is related to the chemical function at R¹. TPMs **5** and **8** have the indole-methyl and isopropyl groups, respectively; while TPM **2** has the *p*-benzoxy-benzyl function. The dramatical increase of inhibitory activity was observed when *p*-benzoxy-benzyl was at R¹, thus suggesting that both, the size and flexibility of chemical group at R¹, are important for the well-fitting of other groups into the interaction site. In addition, *p*-benzoxy-benzyl group increases the hydrophobicity of the compound, which could improve its transport across membranes, a critical step for warranting a higher effective concentration of the compound inside the cell.

2.2.6. Evaluation of the inhibition of the *in vitro* growth of *Escherichia coli*

Finally, the *in vitro* antibacterial activities of the potent and selective ePepN inhibitors **2**, **4** and **11** were evaluated. In this experiment, neither bestatin – used as a positive control for the inhibition of the AP – nor TPMs **4** and **11** inhibited the growth of the cultures of the bacterium *E. coli*, tested up to 100 µM concentration for 3 h, 6 h and 20 h (Fig. 5). There was also no antibacterial activity for compound **16**, the worst ePepN inhibitor of the series (IC₅₀ > 1000 µM; Table 2). In contrast, compound **2** inhibited the *in vitro* growth of *E. coli* with IC₅₀ values lower than 50 µM, at 3 h and 6 h of exposition (Fig. 5A and B), and lower than 100 µM at 20 h (Fig. 5C).

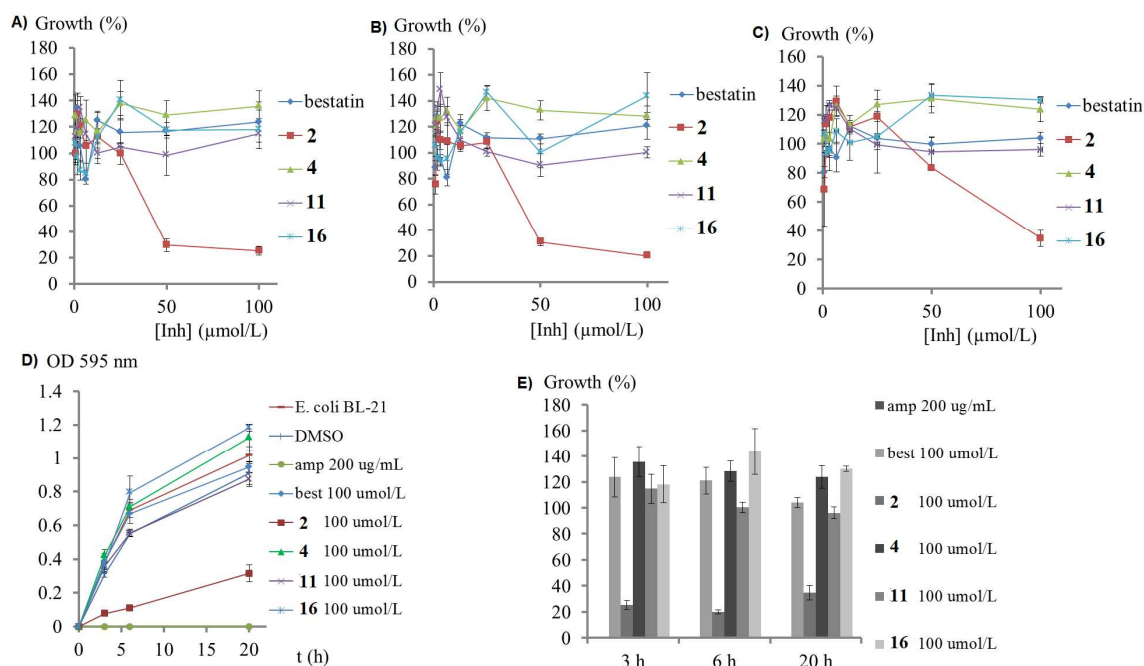


Figure 5. Dose-response studies for the inhibition of the *in vitro* growth of the bacterium *Escherichia coli* BL21 by the TPMs **2**, **4** and **11**. A non-treated bacterial culture and another one exposed to DMSO (vehicle) were used as growth positive controls. The antibiotic ampicillin (amp) was also used as positive control for growth inhibition. Bestatin (best), a known inhibitor of ePepN AP, and TPM **16**, the worst ePepN inhibitor of the series, were tested as well. A), B) and C) Dose-response curves at 3 h (37°C), 6 h (37°C) and 20 h (42°C starting at 6 h), respectively. D) and E) Growth curves of the cultures and comparison of the growth values, respectively, at the higher compound concentrations tested. All data are presented as the mean \pm the standard deviation.

It is intriguing that the two potent ePepN inhibitors showing no *in vitro* inhibition of *E. coli* growth are those derived from tryptophan, *i.e.*, **4** and **11**. A rationale for this result could be that these indole-containing compounds also have other targets in *E. coli*, such as enzymes from tryptophan's metabolic pathways or transporters of this amino acid. This fact would either lead to a reduction of the effective concentrations of **4** and **11** in the cell or transform them into other molecules without inhibitory effect on ePepN. In this sense, metabolic pathways for the synthesis of secondary metabolites of indolic nature have been described

in *E. coli* [73]. On the other hand, the possibility that compound **2** exert its antibacterial effect by a mechanism independent of the ePepN inhibition is also plausible.

2.2.7. Evaluation of the haemolytic activity and cytotoxicity over mammalian cells of selected ePepN inhibitors

As it is shown in Fig. 6, the compounds **2**, **4** and **11** are not potent haemolytic agents. The TPM **11** caused a haemolysis of 15 %, estimated from the haemoglobin release at 20 h of treatment in a concentration of 100 μ M. However, **2** and **4**, in the same conditions, promoted around 40 % of haemolysis. HC₂₀ values representing the compound concentration necessary to reach the 20 % of haemolysis, are shown (Table S1). For none of the compounds it was possible to determine the HC₅₀.

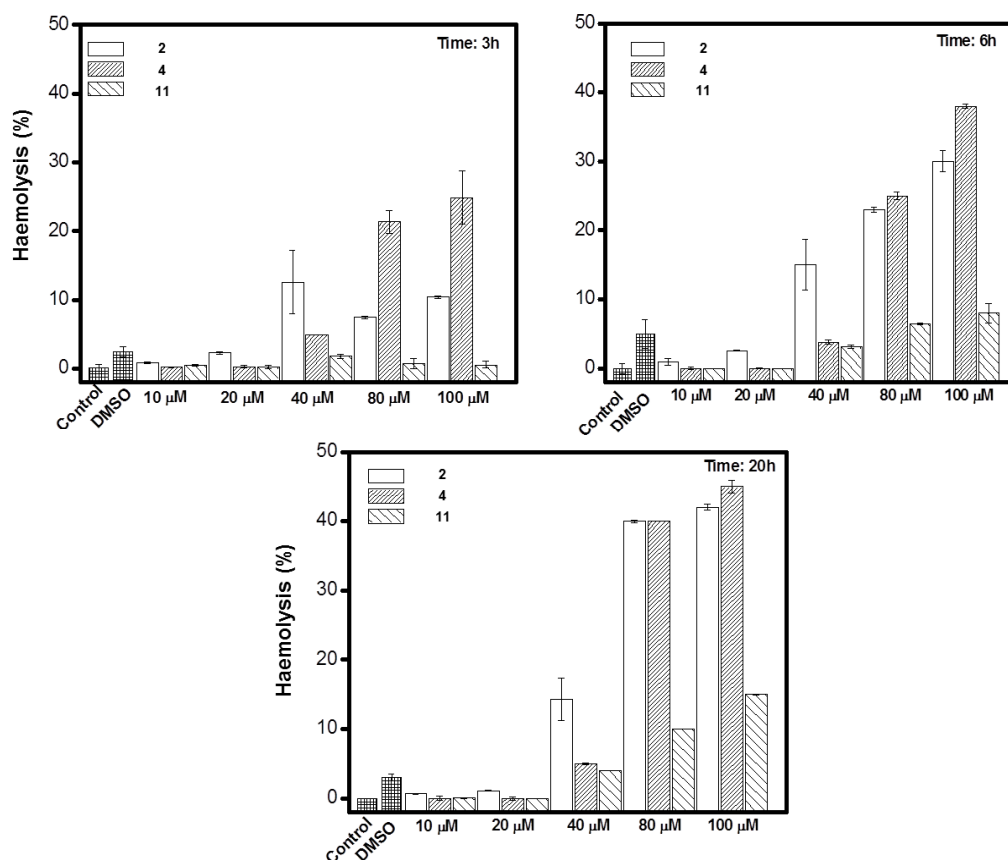


Figure 6. Haemolysis (%) induced at different concentrations of the TPMs at A) 3 h, B) 6 h and C) 20 h after treatment with the indicated doses.

The cytotoxic effect of the three compounds on P3X63Ag cells was further evaluated by MTT assay, which assesses mitochondrial dehydrogenase activity in living cells [74]. As it is shown in Fig. 7, the TPMs **2** and **4** provoked a reduction of the cellular viability from 50 μ M at 3 h of assay (until 60 %), effect that was also observed at 6 and 20 h (until 50 %). However, the compound **11** did not cause a significant decrease of the cellular viability. Determination of IC_{50} , the concentration necessary to kill the 50 % of cells, was only possible for the TPM **2** at 6 and 20 h and **4** at 20 h of treatment, and resulted of 100 μ M (Table S2).

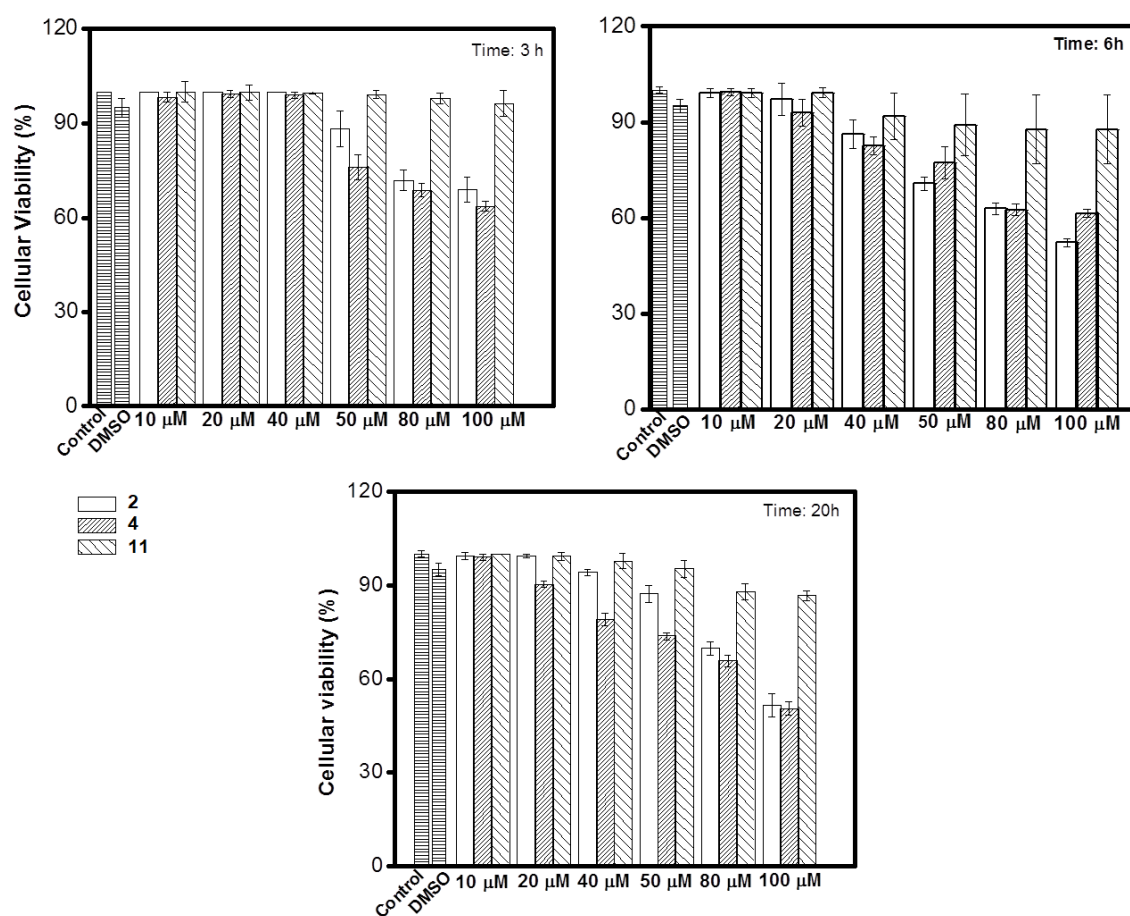


Figure 7. Cytotoxic effect of the TPMs **2**, **4** and **11** on P3X63Ag cells. It is shown the percentage of mitochondrial activity (cellular viability), determined by the reduction of tetrazolium salt (MTT assay) at A) 3 h, B) 6 h and C) 20 h after treatment with the indicated doses of the compounds.

3. Conclusions

We have implemented a solid-phase combinatorial approach based on the Ugi-azide-4CR for the parallel synthesis of TPMs endowed with three centers of diversity generation. 21 different compounds were produced following a simple and reproducible on-resin protocol that enabled the variation of the amino acid, the carbonyl and the isocyanide components taking part in the multicomponent reaction. The screening of the inhibitory activity of the ePepN allowed for the discovery of three potent inhibitors, which also proved high

selectivity for the bacterial enzyme as compared with the mammalian APN ortholog. The structural characteristics of the TPM scaffold favouring a potent ePepN inhibition can be summarized as: *i*) an amino acid moiety with a bulky, hydrophobic aromatic side chain as R^1 , *ii*) a central aromatic substituent as R^2 and *iii*) a bulky aliphatic or aromatic substituent R^3 attached at the tetrazole ring. The most potent TPM **11** showed a non-competitive ($\alpha < 1$) inhibition mode for ePepN, which was suitably explained by combining docking, MD simulations and free energy calculations. In contrast to our original idea, the inhibition mode suggests that there is no coordination of Zn^{2+} in the active site by the tetrazole ring. From the three potent ePepN inhibitors, only compound **2** displayed antibacterial activity *in vitro* toward *E. coli*, indicating that further investigations are needed for developing an effective lead compound based on this antibacterial target. Additionally, none of the three identified inhibitors is a potent haemolytic agent, and only two compounds show moderate cytotoxic activity toward the murine myeloma P3X63Ag cells. In summary, taking into account that ePepN is considered as a model for the rapid identification of microbial APN inhibitors, the new insight provided by this study on the structural-activity relationship and mode of action of this novel class of inhibitor shows prospect for the future development of antimicrobial agents.

4. Experimental section

4.1. Chemistry

4.1.1. Materials and Methods

1H NMR and ^{13}C NMR spectra were recorded at 500/400 MHz and 125/100 MHz on a Bruker/Avance DRX 500 and on a Varian Mercury 400 (400 MHz) at 25°C. Chemical

shifts (δ) are reported in parts per million related to the residual solvent signals, and coupling constants (J) are reported in hertz. High resolution ESI mass spectra were obtained from a Fourier transform ion cyclotron resonance (FT-ICR) mass spectrometer, an RF-only hexapole ion guide and an external electrospray ion source. Solid phase synthesis (SPS) and Ugi-tetrazole-4CR were carried out in Bill-Board-6-pack equipment [51] as a part of the D3 program. Chromatography purification was carried out using cyanosilica cartridges and the purity of the final products was analyzed by HPLC. Analytical HPLC was carried out with the employment of an Agilent 1100/1200 series HPLC equipped with an Agilent 1100/1200 quaternary pump at 25°C, with a flow of 0.800 mL/min and a gradient mixture of A (water + 0.1% FA) and B (acetonitrile + 0.1% FA) from 5 % B to 100 % B in 30 min.

4.1.2. General procedure for the SPS based on Ugi-azide-4CR

The Fmoc α -amino acid (10 eq. relative to the resin) is placed in a round bottom flask with a magnetic stirrer and dissolved in a solution containing DCM (2.5 mL) and some drops of DMF at 0 °C. *N,N*-diisopropylcarbodiimide (DIC) (5 eq., 117 μ L) is then added and the mixture is stirred for 10 min at 0°C. The previous solution is added to the hydroxymethylphenoxy-polystyrene resin (Wang resin, 1.0-1.5 mmol/g) – pre-swollen in DCM and placed in a “Bill-Board-6-pack” apparatus equipped with six 3.5 mL reaction vessels, with screw caps on both ends and a fused frit at one end. Then, 4-dimethylaminopyridine (DMAP) (1 eq., 183 mg) in DMF (0.5 mL) is added to the resin. After 1 h, the resin beads are washed with DCM (3 \times 3 mL), DMF (3 \times 3 mL), and dried each time with the help of an air-push apparatus. The remaining reactive groups on the resin are capped by adding acetic anhydride (5 eq., 708 μ L) and pyridine (1 eq., 121 μ L) in

DMF (2 mL) to the resin (previously swollen in DCM) and then, shaking for 30 additional minutes. The Fmoc deprotection is carried out by treating the pre-washed resin twice with piperidine 20 % in DMF (2 mL) for 10 min. The resin is washed and swollen again with a mixture of THF/MeOH 1:1, then the aldehyde (4 eq.) is added – in the form of piperidinium ion in the case of paraformaldehyde – and the mixture is shaken for 30 min. After washing the resin beads with THF and swelling them again with a mixture of THF/MeOH 1:1, a solution of the isocyanide (4 eq.) and TMSN₃ (4 eq., 792 μL) in THF/MeOH 1:1 is added. The shaking is maintained for 72 h to run the Ugi-azide-4CR to completion. The resin cleavage is performed by adding a mixture of TFA/H₂O/TIS 95:2.5:2.5 (2.5 mL) to the resin beads and shaking for 2 h. The resulting crude product is purified using column chromatography (cyanosilica as stationary phase and *n*-hexane/acetone 3:1 as eluting phase). The pure product is concentrated under reduced pressure, then suspended in water/acetonitrile 4:1 (5 mL) and lyophilized to furnish the TPM.

Compound 1. To a L-Tyr(Bzl)-loaded Wang resin (ca. 0.10 mmol), in a mixture of THF/MeOH 1:1, paraformaldehyde (12 mg, 0.40 mmol) and piperidine (40 μL, 0.40 mmol) and then, cyclohexyl isocyanide (50 μL, 0.40 mmol) and TMSN₃ (53 μL, 0.40 mmol) were added to carry out the on solid phase Ugi-azide-4CR as described in the general procedure. Compound **1** (26 mg, 60 %) was obtained as a light yellow amorphous solid. $R_t = 14.4$ min. ¹H NMR (400 MHz, CDCl₃): $\delta = 1.18 - 1.41$ (m, 2H); 1.41 – 1.56 (m, 1H); 1.57 – 2.33 (m, 7H); 2.84 – 3.02 (m, 1H, CH₂); 3.08 – 3.26 (m, 1H, CH₂); 3.57 – 3.72 (m, 1H, CH); 4.10 – 4.35 (m, 2H, CH₂); 4.50 (tt, 1H, $J = 11.7/ 3.9$ Hz, CH); 4.99 (s, 2H, CH₂ benzyl); 6.83 – 6.92 (m, 2H, 2 × CH, Ar); 7.05 – 7.17 (m, 2H, 2 × CH, Ar); 7.28 – 7.46 (m, 5H, Ar); 8.59 (s, 1H, NH); ¹³C NMR (100 MHz, CDCl₃): $\delta = 25.0, 25.3, 33.3$ (CH₂); 59.0 (CH); 70.2

(CH₂); 115.2, 127.6, 128.1, 128.7 (CH); 128.8 (C); 130.5 (CH); 137.0 (C), 140.7 (CH).
ESI-MS: $m/z = 458.4 [M+Na]^+$; $893.5 [2M+Na]^+$ (calculated for C₂₄H₂₉N₅NaO₃: 458.2).
HRMS: $m/z = 436.2336 [M + H]^+$ (calculated for C₂₄H₂₈N₅O₃: 434.2192)

Compound 2. To a L-Tyr(Bzl)-loaded Wang resin (ca. 0.10 mmol), in a mixture of THF/MeOH 1:1, *p*-methoxybenzaldehyde (49 μ L, 0.40 mmol) and then, cyclohexylisocyanide (50 μ L, 0.40 mmol) and TMSN₃ (53 μ L, 0.40 mmol) were added to carry out the on solid phase Ugi-azide-4CR as described in the general procedure. Compound **2** (45 mg, 83 %) was obtained as a light yellow solid. $R_t = 17.9$ min. A mixture of diastereomers in a 2:1 ratio was observed by NMR. ¹H NMR (400 MHz, CDCl₃): $\delta = 1.01 - 1.42$ (m, 5H); $1.58 - 1.91$ (m, 5H); 2.78 (dd, 1H, $J = 14.0/9.8$ Hz, CH₂); 3.21 (dd, 1H, $J = 14.0/4.0$ Hz, CH₂); 3.42 (dd, 1H, $J = 9.8/4.0$ Hz, CH); 3.77 (s, 3H, OCH₃); $3.82 - 3.95$ (m, 1H); 4.82 (s, 1H); 5.08 (s, 2H, CH₂ benzyl); 6.73 (d, 1H, $J = 8.6$ Hz, CH, Ar); $6.81 - 6.93$ (m, 4H, Ar); 7.07 (d, 2H, $J = 8.5$ Hz, 2 \times CH, Ar); $7.13 - 7.22$ (m, 1H); $7.30 - 7.49$ (m, 5H, Ar). ¹³C NMR (100 MHz, CDCl₃): $\delta = 24.8, 25.32, 25.32, 38.1$ (CH₂); 55.5 (CH₃); $56.4, 58.3, 60.4$ (CH); 70.3 (CH₂); $114.7, 115.4, 127.5, 128.8, 129.0$ (CH); 129.2 (C); 130.5 (CH); $137.1, 154.9, 158.1, 160.0, 160.2$ (C); 174.7 (C=O). HRMS: $m/z = 542.2754 [M + H]^+$ (calculated for C₃₁H₃₆N₅O₄: 542.2767); $1083.5437 [2M + H]^+$ (calculated for C₆₂H₇₁N₁₀O₈: 1083.5456).

Compound 3. To a L-Trp-loaded Wang resin (ca. 0.1 mmol), in a mixture of THF/MeOH 1:1, paraformaldehyde (12 mg, 0.40 mmol) and piperidine (40 μ L, 0.40 mmol) and then, cyclohexyl isocyanide (50 μ L, 0.40 mmol) and TMSN₃ (53 μ L, 0.40 mmol) were added to carry out the on solid phase Ugi-azide-4CR as described in the general procedure. Compound **3** (24 mg, 65 %) was obtained as a dark yellow solid $R_t = 11.6$ min. ¹H NMR

(400 MHz, CD₃OD): δ = 1.13 – 1.19 (m, 1H); 1.21 – 1.46 (m, 3H); 1.65 – 1.98 (m, 6H); 3.19 (dd, 1H, J = 14.8/ 8.2 Hz); 3.38 (dd, 1H, J = 14.8/ 4.6 Hz); 3.58 – 3.72 (m, 1H); 3.83 (dd, 1H, J = 8.1/ 4.8 Hz); 4.15 (d, 1H, J = 14.9 Hz); 4.27 (d, 1H, J = 14.9 Hz); 7.02 (ddd, 1H, J = 8.0/ 7.0/ 1.1 Hz, Ar); 7.11 (ddd, 1H, J = 8.0/ 7.0/1.1 Hz, Ar); 7.15 (s, 1H, Ar); 7.36 (d, 1H, J = 8.0 Hz, Ar); 7.58 (d, 1H, J = 8.0 Hz, Ar). HRMS: m/z = 369.2029 [M + H]⁺ (calculated for C₁₉H₂₅N₆O₂: 369.2039).

Compound 4. To a L-Trp-loaded Wang resin (ca. 0.1 mmol), in a mixture of THF/MeOH 1:1, 2-furaldehyde (33 μ L, 0.40 mmol) and then, cyclohexyl isocyanide (50 μ L, 0.40 mmol) and TMSN₃ (53 μ L, 0.40 mmol) were added to carry out the on solid phase Ugi-azide-4CR as described in the general procedure. Compound **4** (31 mg, 73 %) was obtained as a light yellow solid. R_t = 15.0 min. A mixture of diastereomers in a 1:1 ratio was observed by NMR. ¹H NMR (400 MHz, CDCl₃): δ = 1.12 – 1.30 (m, 3H); 1.47 – 1.58 (m, 1H); 1.64 – 1.91 (m, 6H); 3.12 (dd, 1H, J = 14.6/ 8.4 Hz, CH₂); 3.38 (dd, 1H, J = 14.6/ 4.5 Hz, CH₂); 3.72 (dd, 1H, J = 8.4/ 4.5 Hz, CH); 4.27 – 4.37 (m, 1H); 5.30 (s, 1H); 6.09 (d, 1H, J = 3.1 Hz, Ar); 6.18 – 6.23 (m, 1H, Ar); 7.03 – 7.23 (m, 3H, Ar); 7.30 (s, 1H, Ar); 7.35 (dd, 1H, J = 7.9/ 5.2 Hz, Ar); 7.49 (d, 1H, J = 7.9 Hz, Ar); 8.36 (s, 1H, NH). ¹³C NMR (100 MHz, CDCl₃): δ = 24.9, 25.3, 29.0, 32.7 (CH₂); 50.3 (CH₃); 50.6, 58.7, 59.7, 108.9; 110.0 (CH); 110.1 (C); 110.9, 111.6, 118.7, 119.8, 122.4 (CH), 127.6, 136.4 (C); 143.3 (CH); 149.5, 152.2 (C); 175.7 (C=O). HRMS: m/z = 435.2131 [M+H]⁺ (calculated for C₂₃H₂₇N₆O₃: 435.2145); 869.4201 [2M+H]⁺ (calculated for C₄₆H₅₃N₁₂O₆: 869.4211).

Compound 5. To a L-Trp-loaded Wang resin (ca. 0.1 mmol), in a mixture of THF/MeOH 1:1, *p*-methoxybenzaldehyde (49 μ L, 0.40 mmol) and then, cyclohexyl isocyanide (50 μ L, 0.40 mmol) and TMSN₃ (53 μ L, 0.40 mmol) were added to carry out the on solid phase

Ugi-azide-4CR as described in the general procedure. Compound **5** (40 mg, 83 %) was obtained as a light yellow solid. $R_t = 15.1/15.3$ min. A mixture of diastereomers in a 1.4:1 ratio was observed by NMR. ^1H NMR (400 MHz, CD_3OD): $\delta = 0.93 - 1.08$ (m, 1H); 1.07 – 1.45 (m, 4H); 1.46 – 1.86 (m, 6H); 3.05 (dd, 1H, $J = 14.4/9.4$ Hz); 3.39 (dd, 1H, $J = 14.4/4.1$ Hz); 3.61 (dd, 1H, $J = 9.4/4.1$ Hz); 3.73 (s, 3H, OCH_3); 3.98 – 4.08 (m, 1H); 5.15 (s, 1H); 6.66 (d, 2H, $J = 8.4$ Hz, Ar); 6.83 – 6.92 (m, 2H, Ar); 7.15 (d, 1H, $J = 7.9$ Hz, Ar); 7.18 (s, 1H, Ar); 7.41 (d, 2H, $J = 8.4$ Hz, Ar); 7.61 (d, 1H, $J = 7.9$ Hz, Ar). ^{13}C NMR (100 MHz, CD_3OD): $\delta = 25.9, 26.2, 30.0, 33.7$ (CH_2); 55.7 (CH_3); 56.2, 59.1, 60.8 (CH); 111.1 (C); 112.5, 115.3, 119.4, 120.0, 122.7, 124.7 (CH); 128.4 (C); 130.1 (CH), 138.3, 155.6, 161.4 (C); 176.5 (C=O). HRMS: $m/z = 475.2442$ [$\text{M} + \text{H}$] $^+$ (calculated for $\text{C}_{26}\text{H}_{31}\text{N}_6\text{O}_3$: 475.2458); 949.4819 [$2\text{M} + \text{H}$] $^+$ (calculated for $\text{C}_{52}\text{H}_{61}\text{N}_{12}\text{O}_6$: 949.4837).

Compound 6. To a L-Trp-loaded Wang resin (ca. 0.1 mmol), in a mixture of THF/MeOH 1:1, imidazole-2-carbaldehyde (39 μL , 0.40 mmol) and then, cyclohexyl isocyanide (50 μL , 0.40 mmol) and TMSN_3 (53 μL , 0.40 mmol) were added to carry out the on solid phase Ugi-azide-4CR as described in the general procedure. Compound **6** (26 mg, 60 %) was obtained as a light yellow solid. $R_t = 10.3/10.6$ min. A mixture of diastereomers in a 1:1 ratio was observed by NMR. ^1H NMR (400 MHz, CD_3OD): $\delta = 1.10 - 1.52$ (m, 3H); 1.57 – 1.91 (m, 7H); 1.98 (d, 1H, $J = 8.8$ Hz); 3.04 (dd, 1H, $J = 14.6/8.5$ Hz); 3.60 – 3.65 (m, 1H); 3.75 (dd, 1H, $J = 8.5/4.5$ Hz); 4.31 – 4.42 (m, 1H); 5.48 (s, 1H); 5.88 (s, 1H); 6.91 – 7.02 (m, 1H, Ar); 7.05 – 7.14 (m, 2H, Ar); 7.31 – 7.39 (m, 2H, Ar); 7.45 (d, 1H, $J = 8.0$ Hz, Ar); 7.51 (d, 1H, $J = 7.9$ Hz, Ar). ^{13}C NMR (100 MHz, CD_3OD): $\delta = 26.0, 29.9, 33.8, 34.1$ (CH_2); 49.0 (CH); 49.3 (CH_3); 59.6 (CH); 110.3 (C); 112.5, 119.2, 120.0, 121.2, 121.0, 122.6, 124.9 (CH); 128.5, 138.2, 145.0, 152.5 (C); 175.9 (C=O). HRMS: $m/z = 435.2240$

$[M + H]^+$ (calculated for $C_{22}H_{27}N_8O_2$: 435.2257); 869.4421 $[2M + H]^+$ (calculated for $C_{44}H_{53}N_{16}O_4$: 869.4436).

Compound 7. To a L-Trp-loaded Wang resin (ca. 0.1 mmol), in a mixture of THF/MeOH 1:1, 3-pyridincarbalddehyde (38 μ L, 0.40 mmol) and then, cyclohexyl isocyanide (50 μ L, 0.40 mmol) and $TMSN_3$ (53 μ L, 0.40 mmol) were added to carry out the on solid phase Ugi-azide-4CR as described in the general procedure. Compound **7** (36 mg, 81 %) was obtained as a light yellow solid. $R_t = 11.2/12.1$ min. A mixture of diastereomers in a 1.7:1 ratio was observed by NMR. 1H NMR (400 MHz, CD_3OD): $\delta = 1.12 - 1.43$ (m, 3H); 1.47 - 2.10 (m, 8H); 3.07 (dd, 1H, $J = 14.5/8.5$ Hz); 3.27 (dd, 1H, $J = 14.5/4.7$ Hz); 3.60 (dd, 1H, $J = 8.5/4.7$ Hz); 4.31 - 4.44 (m, 1H); 5.59 (s, 1H); 7.02 (t, 1H, $J = 7.4$ Hz, Ar); 7.08 - 7.18 (m, 3H, Ar); 7.37 (d, 1H, $J = 8.3$ Hz, Ar); 7.53 (d, 1H, $J = 7.8$ Hz, Ar); 7.61 (dd, 1H, $J = 8.0/5.3$ Hz, Ar); 8.17 (d, 1H, $J = 8.0$ Hz, Ar); 8.56 (d, 1H, $J = 5.3$ Hz, Ar), 8.70 (s, 1H). ^{13}C NMR (100 MHz, CD_3OD): $\delta = 25.9, 26.1, 33.6, 33.9$ (CH_2); 49.3 (CH); 59.3, 60.7 (CH); 111.5 (C); 112.6, 119.3, 119.9, 122.6, 124.6, 126.5 (CH); 128.7, 138.1, 138.2 (C); 142.5, 144.9, 146.2 (CH), 154.8 (C); 177.0 ($C=O$). HRMS: $m/z = 446.2286$ $[M + H]^+$ (calculated for $C_{24}H_{28}N_7O_2$: 446.2304); 891.4513 $[2M + H]^+$ (calculated for $C_{48}H_{55}N_{14}O_4$: 891.4531).

Compound 8. To a L-Val-loaded Wang resin (ca. 0.1 mmol), in a mixture of THF/MeOH 1:1, *p*-methoxybenzaldehyde (49 μ L, 0.40 mmol) and then, cyclohexyl isocyanide (50 μ L, 0.40 mmol) and $TMSN_3$ (53 μ L, 0.40 mmol) were added to carry out the on solid phase Ugi-azide-4CR as described in the general procedure. Compound **8** (31 mg, 80 %) was obtained as a white solid. $R_t = 14.6/14.9$ min. A mixture of diastereomers in a 3:1 ratio was observed by NMR. 1H NMR (400 MHz, CD_3OD): $\delta = 0.97$ (d, 3H, $J = 6.7$ Hz, CH_3); 0.99 (d, 3H, $J = 6.8$ Hz, CH_3); 1.13 - 1.39 (m, 2H); 1.41 - 1.54 (m, 1H); 1.66 - 1.98 (m, 8H);

1.98 – 2.13 (m, 1H); 3.02 (d, 1H, $J = 5.1$ Hz, CH); 3.81 (s, 3H, OCH₃); 4.55 – 4.65 (m, 1H); 5.27 (s, 1H); 6.97 (d, 2H, $J = 8.7$ Hz, Ar); 7.38 (d, 2H, $J = 8.7$ Hz, Ar). ¹³C NMR (100 MHz, CD₃OD): $\delta = 18.6, 19.8$ (CH₃); 26.1, 26.3 (CH₂); 32.5 (CH); 33.8 (CH₂); 55.9 (CH₃); 56.6, 59.2, 65.0, 115.4 (CH), 130.0 (C), 130.7 (CH), 156.8, 161.6 (C); 176.9 (C=O). HRMS: $m/z = 388.2340$ [M + H]⁺ (calculated for C₂₀H₃₀N₅O₃: 388.2349); 775.4602 [2M + H]⁺ (calculated for C₄₀H₅₉N₁₀O₆: 775.4619).

Compound 9. To a L-Val-loaded Wang resin (ca. 0.1 mmol), in a mixture of THF/MeOH 1:1, imidazole-2-carbaldehyde (39 μ L, 0.40 mmol) and then, cyclohexyl isocyanide (50 μ L, 0.40 mmol) and TMSN₃ (53 μ L, 0.40 mmol) were added to carry out the on solid phase Ugi-azide-4CR as described in the general procedure. Compound **9** (24 mg, 68 %) was obtained as a dark yellow solid. $R_t = 13.0/13.4$ min. A mixture of diastereomers in a 2:1 ratio was observed by NMR. ¹H NMR (400 MHz, CD₃OD): $\delta = 0.92$ (d, 3H, $J = 7.2$ Hz, CH₃); 0.94 (d, 3H, $J = 7.0$ Hz, CH₃); 1.27 – 1.52 (m, 1H); 1.43 – 1.65 (m, 2H); 1.72 – 1.84 (m, 1H); 1.86 – 2.27 (m, 7H); 3.21 (d, 1H, $J = 4.8$ Hz, CH); 4.67 – 4.79 (m, 1H); 5.93 (s, 1H); 7.54 (s, 2H, Ar). ¹³C NMR (100 MHz, CD₃OD): $\delta = 18.3, 19.8$ (CH₃); 26.0, 26.2 (CH₂); 33.0 (CH); 34.2 (CH₂); 59.7, 66.0, 121.1, 121.4 (CH); 145.5, 152.4 (C); 176.3 (C=O). HRMS: $m/z = 348.2133$ [M + H]⁺ (calculated for C₁₆H₂₆N₇O₂: 348.2148); 695.4195 [2M + H]⁺ (calculated for C₃₂H₅₁N₁₄O₄: 695.4218).

Compound 10. To a L-Val-loaded Wang resin (ca. 0.1 mmol), in a mixture of THF/MeOH 1:1, 3-pyridincarbalddehyde (38 μ L, 0.40 mmol) and then, cyclohexyl isocyanide (50 μ L, 0.40 mmol) and TMSN₃ (53 μ L, 0.40 mmol) were added to carry out the on solid phase Ugi-azide-4CR as described in the general procedure. Compound **10** (25 mg, 68 %) was obtained as a dark yellow solid. $R_t = 11.0$ min. A mixture of diastereomers in a 3:1 ratio

was observed by NMR. ^1H NMR (400 MHz, CD_3OD): $\delta = 0.97$ ($2 \times \text{d}$, $2 \times 3\text{H}$, $J = 6.8$ Hz, $2 \times \text{CH}_3$); 1.29 – 1.43 (m, 1H); 1.49 – 1.64 (m, 2H); 1.74 – 2.19 (m, 8H); 2.99 (d, 1H, $J = 4.9$ Hz); 5.00 – 5.11 (m, 1H); 5.46 (s, 1H); 7.74 (dd, 1H, $J = 7.9/ 5.1$ Hz, Ar); 8.32 (dt, 1H, $J = 8.0/ 2.0$ Hz, Ar); 8.68 (d, 1H, $J = 5.1$ Hz, Ar); 8.84 (d, 1H, $J = 2.0$ Hz, Ar). ^{13}C NMR (100 MHz, CD_3OD): $\delta = 18.3, 19.7$ (CH_3); 26.2, 26.3 (CH_2); 32.5 (CH); 34.0, 34.2 (CH_2); 54.1, 59.1, 65.3, 126.7 (CH), 137.9 (C); 141.9, 147.9, 148.0 (CH); 155.8 (C); 176.5 (C=O). $\text{dr} = 60.00$. HRMS: $m/z = 359.2184$ [$\text{M} + \text{H}$] $^+$ (calculated for $\text{C}_{18}\text{H}_{27}\text{N}_6\text{O}_2$: 359.2195); 717.4295 [$2\text{M} + \text{H}$] $^+$ (calculated for $\text{C}_{36}\text{H}_{53}\text{N}_{12}\text{O}_4$: 717.4313).

Compound 11. To a L-Trp-loaded Wang resin (ca. 0.1 mmol), in a mixture of THF/MeOH 1:1, 2-furaldehyde (33 μL , 0.40 mmol) and then, benzyl isocyanide (49 μL , 0.40 mmol) and TMSN_3 (53 μL , 0.40 mmol) were added to carry out the on solid phase Ugi-azide-4CR as described in the general procedure. Compound **11** (37 mg, 83 %) was obtained as a light brown solid. $R_t = 14.3$ min. A mixture of diastereomers in a 1.4:1 ratio was observed by NMR. ^1H NMR (400 MHz, CDCl_3): $\delta = 3.03$ (dd, 1H, $J = 14.8/ 7.5$ Hz, CH_2); 3.18 (dd, 1H, $J = 14.8/ 4.7$ Hz, CH_2); 3.44 (dd, 1H, $J = 7.5/ 4.7$ Hz, CH_2); 5.01 (d, 1H, $J = 15.5$ Hz, CH_2); 5.19 (d, 1H, $J = 15.5$ Hz, CH_2); 5.30 (s, 1H); 5.94 (d, 1H, $J = 3.0$ Hz, Ar); 6.03 (d, 1H, $J = 3.0$ Hz, Ar); 6.82 (m, 1H, Ar); 6.95 – 7.28 (m, 8H, Ar); 7.35 (d, 1H, $J = 8.0$ Hz, Ar); 7.53 (d, 1H, $J = 8.0$ Hz, Ar); 8.27 (s, 1H, NH). ^{13}C NMR (100 MHz, CDCl_3): $\delta = 28.7$ (CH_2); 50.7 (CH); 51.1 (CH_2), 59.7, 109.4; 110.8, 111.6, 118.7, 119.9, 122.5, 123.6 (CH); 127.2 (C); 127.4 (CH); 127.5 (C); 128.7, 129.0 (CH); 133.3, 136.4 (C); 143.4 (CH), 148.7, 153.2 (C); 175.8 (C=O). HRMS: $m/z = 443.1819$ [$\text{M} + \text{H}$] $^+$ (calculated for $\text{C}_{24}\text{H}_{23}\text{N}_6\text{O}_3$: 443.1832); 885.3577 [$2\text{M} + \text{H}$] $^+$ (calculated for $\text{C}_{48}\text{H}_{45}\text{N}_{12}\text{O}_6$: 885.3585).

Compound 12. To a L-Trp-loaded Wang resin (ca. 0.1 mmol), in a mixture of THF/MeOH 1:1, *p*-methoxybenzaldehyde (49 μ L, 0.40 mmol) and then, benzyl isocyanide (49 μ L, 0.40 mmol) and TMSN₃ (53 μ L, 0.40 mmol) were added to carry out the on solid phase Ugi-azide-4CR as described in the general procedure. Compound **12** (39 mg, 80 %) was obtained as a light yellow solid. R_t = 14.1/14.4 min. A mixture of diastereomers in a 1.1:1 ratio was observed by NMR. ¹H NMR (400 MHz, CD₃OD): δ = 1.15 (d, 1H, J = 5.9 Hz); 3.00 (dd, 1H, J = 14.3/ 9.6 Hz); 3.37 – 3.42 (m, 1H); 3.52 (dd, 1H, J = 9.5/ 4.1 Hz); 3.68 (s, 3H, OCH₃); 5.10 (s, 1H); 5.17 (d, 1H, J = 15.7 Hz); 5.29 (d, 1H, J = 15.7 Hz); 6.53 (d, 2H, J = 8.2 Hz, Ar); 6.62 – 6.70 (m, 2H, Ar); 6.88 (d, 1H, J = 7.1 Hz, Ar); 6.93 – 6.99 (m, 1H, Ar); 7.02 – 7.29 (m, 5H, Ar); 7.35 – 7.45 (m, 2H, Ar); 7.57 (d, 1H, J = 7.9 Hz); 8.28 (s, 1H, NH). ¹³C NMR (100 MHz, CD₃OD): δ = 30.0 (CH₂); 51.7 (CH₂); 55.6 (CH₃); 56.5, 61.2 (CH); 111.1 (C); 112.5, 115.1, 119.4, 120.0, 122.7, 125.0, 128.1 (CH); 128.5 (C); 128.6, 129.8, 130.1 (CH); 134.6, 135.1, 138.3, 157.3, 161.2 (C); 176.9 (C=O). HRMS: m/z = 483.2129 [M + H]⁺ (calculated for C₂₇H₂₇N₆O₃: 483.2145); 965.4193 [2M + H]⁺ (calculated for C₅₄H₅₃N₁₂O₆: 965.4211).

Compound 13. To a L-Trp-loaded Wang resin (ca. 0.1 mmol), in a mixture of THF/MeOH 1:1, imidazole-2-carbaldehyde (39 μ L, 0.40 mmol) and then, benzyl isocyanide (49 μ L, 0.40 mmol) and TMSN₃ (53 μ L, 0.40 mmol) were added to carry out the on solid phase Ugi-azide-4CR as described in the general procedure. Compound **13** (31 mg, 69 %) was obtained as a red-brown solid. R_t = 10.0/10.2 min. A mixture of diastereomers in a 1.6:1 ratio was observed by NMR. ¹H NMR (400 MHz, CD₃OD): δ = 2.87 – 3.01 (m, 1H); 3.21 (dd, 1H, J = 12.1/ 3.8 Hz); 3.63 (dd, 1H, J = 9.3/ 3.8 Hz); 5.03 (d, 1H, J = 15.3 Hz); 5.24 (d, 1H, J = 15.3 Hz); 5.54 (s, 1H); 6.76 (d, 1H, J = 7.2 Hz, Ar); 6.88 – 7.01 (m, 2H, Ar);

7.01 – 7.12 (m, 1H; Ar); 7.12 – 7.37 (m, 7H, Ar); 7.48 (d, 1H, $J = 7.9$ Hz, NH). ^{13}C NMR (100 MHz, CD_3OD): $\delta = 30.8, 52.1$ (CH_2); 59.6, 62.2 (CH); 110.7 (C); 112.7, 119.3, 120.1, 121.0, 122.7, 124.9 (CH); 128.2 (C); 128.8, 129.2, 129.7, 130.0 (CH), 134.6, 135.3, 138.2, 153.0 (C); 176.2 (C=O). HRMS: $m/z = 443.1926$ [$\text{M} + \text{H}$] $^+$ (calculated for $\text{C}_{23}\text{H}_{23}\text{N}_8\text{O}_2$: 443.1944); 885.3789 [$2\text{M} + \text{H}$] $^+$ (calculated for $\text{C}_{46}\text{H}_{45}\text{N}_{16}\text{O}_4$: 885.3810).

Compound 14. To a L-Val-loaded Wang resin (ca. 0.1 mmol), in a mixture of THF/MeOH 1:1, paraformaldehyde (12 mg, 0.40 mmol) and piperidine (40 μL , 0.40 mmol) and then, benzyl isocyanide (49 μL , 0.40 mmol) and TMSN_3 (53 μL , 0.40 mmol) were added to carry out the on solid phase Ugi-azide-4CR as described in the general procedure. Compound **14** (18 mg, 61 %) was obtained as a light yellow solid. $R_t = 10.6$ min. ^1H NMR (400 MHz, CD_3OD): $\delta = 0.94$ (d, 6H, $J = 6.6$ Hz, $2 \times \text{CH}_3$); 1.94 – 2.11 (m, 1H, CH); 3.16 (d, 1H, $J = 4.9$ Hz, CH); 4.03 (d, 1H, $J = 14.9$ Hz, CH_2); 4.20 (d, 1H, $J = 14.9$ Hz, CH_2); 5.74 (d, 1H, $J = 15.4$ Hz, CH_2 benzyl); 5.79 (d, 1H, $J = 15.1$ Hz, CH_2 benzyl); 7.29 – 7.40 (m, 5H, Ar); ^{13}C NMR (100 MHz, CD_3OD): $\delta = 18.7, 19.4$ (CH_3); 32.1 (CH); 41.5, 52.0 (CH_2); 67.8, 129.1, 129.8, 130.1 (CH); 135.4, 154.1 (C); 175.9 (C=O). HRMS: $m/z = 304.1763$ [$\text{M}(\text{MeOH}) + \text{H}$] $^+$ (calculated for $\text{C}_{15}\text{H}_{22}\text{N}_5\text{O}_2$: 304.1773); 607.3457 [$2\text{M}(\text{MeOH}) + \text{H}$] $^+$ (calculated for $\text{C}_{30}\text{H}_{43}\text{N}_{10}\text{O}_4$: 607.3469).

Compound 15. To a L-Val-loaded Wang resin (ca. 0.1 mmol), in a mixture of THF/MeOH 1:1, imidazole-2-carbaldehyde (39 μL , 0.40 mmol) and then, benzyl isocyanide (49 μL , 0.40 mmol) and TMSN_3 (53 μL , 0.80 mmol) were added to carry out the on solid phase Ugi-azide-4CR as described in the general procedure. Compound **15** (23 mg, 64 %) was obtained as a dark yellow solid. $R_t = 8.9/9.1$ min. A mixture of diastereomers in a 1.6:1 ratio was observed by NMR. ^1H NMR (400 MHz, CD_3OD): $\delta = 0.85$ (d, 3H, $J = 5.7$ Hz, CH_3);

0.88 (d, 3H, $J = 6.3$ Hz, CH_3); 1.90 – 2.07 (m, 1H); 3.11 (d, 1H, $J = 4.8$ Hz, CH); 5.48 (s, 1H); 5.79 (d, 1H, $J = 10.9$ Hz); 5.91 (d, 1H, $J = 10.9$ Hz); 7.21 – 7.41 (m, 6H, Ar); 7.46 (s, 1H, Ar). ^{13}C NMR (100 MHz, CD_3OD): $\delta = 18.3, 19.5$ (CH_3); 33.0, 50.4 (CH); 52.5 (CH_2); 65.0, 65.9, 121.3, 121.6, 128.7, 129.2, 129.8, 130.2 (CH), 135.2, 144.8, 155.4 (C); 176.1 (C=O). HRMS: $m/z = 356.1825$ [$M + H$] $^+$ (calculated for $C_{17}H_{22}N_7O_2$: 356.1835); 711.3578 [$2M + H$] $^+$ (calculated for $C_{34}H_{43}N_{14}O_4$: 711.3592).

Compound 16. To a L-Val-loaded Wang resin (ca. 0.1 mmol), in a mixture of THF/MeOH 1:1, *p*-methoxybenzaldehyde (49 μ L, 0.40 mmol) and then, benzyl isocyanide (49 μ L, 0.40 mmol) and $TMSN_3$ (53 μ L, 0.40 mmol) were added to carry out the on solid phase Ugi-azide-4CR as described in the general procedure. Compound **16** (29 mg, 73 %) was obtained as a light yellow syrup. $R_t = 16.4/16.8$ min. A mixture of diastereomers in a 3:1 ratio was observed by NMR. 1H NMR (400 MHz, CD_3OD): $\delta = 0.89$ (d, 3H, $J = 6.9$ Hz, CH_3); 0.92 (d, 3H, $J = 6.9$ Hz, CH_3); 1.88 – 2.01 (m, 1H); 2.95 (d, 1H, $J = 5.7$ Hz); 3.78 (s, 3H, OCH_3); 5.10 (s, 1H); 5.60 (d, 1H, $J = 15.6$ Hz); 5.67 (d, 1H, $J = 15.6$ Hz); 6.85 (d, 2H, $J = 8.7$ Hz, Ar); 7.02 – 7.10 (m, 2H); 7.19 (d, 2H, $J = 8.7$ Hz, Ar); 7.24 – 7.37 (m, 3H, Ar). ^{13}C NMR (100 MHz, CD_3OD): $\delta = 18.8, 19.6$ (CH_3); 32.7 (CH); 51.9 (CH_2); 55.8 (CH_3); 56.4, 65.4, 115.2, 128.6, 129.5, 129.9, 130.6 (CH); 135.5, 157.9, 161.4 (C); 176.1 (C=O). HRMS: $m/z = 410.2176$ [M (OMe) + H] $^+$ (calculated for $C_{22}H_{28}N_5O_3$: 410.2192); 819.4282 [$2(M(OMe)) + H$] $^+$ (calculated for $C_{44}H_{55}N_{10}O_6$: 819.4306).

Compound 17. To a L-Val-loaded Wang resin (ca. 0.1 mmol), in a mixture of THF/MeOH 1:1, paraformaldehyde (12 mg, 0.40 mmol) and piperidine (40 μ L, 0.40 mmol) and then, 3-phenylpropyl isocyanide (68 μ L, 0.40 mmol) and $TMSN_3$ (53 μ L, 0.40 mmol) were added to carry out the on solid phase Ugi-azide-4CR as described in the general procedure.

Compound **17** (20 mg, 63 %) was obtained as a white solid. $R_t = 15.5$ min. ^1H NMR (400 MHz, CD_3OD): $\delta = 0.95$ (d, 3H, $J = 6.3$ Hz, CH_3); 0.96 (d, 3H, $J = 5.3$ Hz, CH_3); 1.98 – 2.08 (m, 1H); 2.31 (p, 2H, $J = 7.5$ Hz, CH_2); 2.73 (t, 2H, $J = 7.5$ Hz, CH_2); 3.09 (d, 1H, $J = 5.0$ Hz, CH); 4.06 (d, 1H, $J = 14.6$ Hz, CH_2); 4.20 (d, 1H, $J = 14.6$ Hz, CH_2); 4.47 – 4.56 (m, 2H); 7.17 – 7.26 (m, 3H, Ar); 7.30 (t, $J = 7.5$ Hz, Ar). ^{13}C NMR (100 MHz, CD_3OD): $\delta = 18.6, 19.7$ (CH_3); 31.9 (CH_2); 32.3 (CH); 33.5, 41.5, 48.1 (CH_2); 68.0, 127.3, 129.5, 129.6 (CH), 141.8, 154.5 (C); 176.5 (C=O). HRMS: $m/z = 318.1917$ [$\text{M} + \text{H}$] $^+$ (calculated for $\text{C}_{16}\text{H}_{24}\text{N}_5\text{O}_2$: 318.1930); 635.3766 [$2\text{M} + \text{H}$] $^+$ (calculated for $\text{C}_{32}\text{H}_{47}\text{N}_{10}\text{O}_4$: 635.3782).

Compound 18. To a L-Val-loaded Wang resin (ca. 0.1 mmol), in a mixture of THF/MeOH 1:1, *p*-methoxybenzaldehyde (49 μL , 0.40 mmol) and then, 3-phenylpropyl isocyanide (68 μL , 0.40 mmol) and TMSN_3 (53 μL , 0.40 mmol) were added to carry out the on solid phase Ugi-azide-4CR as described in the general procedure. Compound **18** (36 mg, 85 %) was obtained as a light yellow solid. $R_t = 14.9/15.4$ min. A mixture of diastereomers in a 3.4:1 ratio was observed by NMR. ^1H NMR (400 MHz, CD_3OD): $\delta = 0.94$ (d, 3H, $J = 6.9$ Hz, CH_3); 0.97 (d, 3H, $J = 7.0$ Hz, CH_3); 1.78 – 2.07 (m, 4H); 2.43 – 2.63 (m, 2H, CH_2); 2.98 (d, 1H, $J = 5.0$ Hz, CH); 3.79 (s, 3H, OCH_3); 4.31 (t, 2H, $J = 7.6$ Hz, CH_2); 5.17 (s, 1H); 6.92 (d, 2H, $J = 8.6$ Hz, Ar); 7.12 (d, 2H, $J = 7.2$ Hz, Ar); 7.17 – 7.32 (m, 5H, Ar). ^{13}C NMR (100 MHz, CD_3OD): $\delta = 18.6, 19.7$ (CH_3); 31.9 (CH_2); 32.4 (CH); 33.4, 48.1 (CH_2); 55.8 (CH_3); 57.4, 64.9, 115.5, 127.3, 129.5, 129.6 (CH); 130.1 (C); 130.8 (CH); 141.7, 157.2, 161.7 (C); 176.7 (C=O). HRMS: $m/z = 424.2349$ [$\text{M} + \text{H}$] $^+$ (calculated for $\text{C}_{23}\text{H}_{30}\text{N}_5\text{O}_3$: 424.2349); 438.2491 [$\text{M}(\text{OMe}) + \text{H}$] $^+$ (calculated for $\text{C}_{24}\text{H}_{32}\text{N}_5\text{O}_3$: 438.2505); 847.4603 [$2\text{M} + \text{H}$] $^+$ (calculated for $\text{C}_{46}\text{H}_{59}\text{N}_{10}\text{O}_6$: 847.4619).

Compound 19. To a L-Val-loaded Wang resin (ca. 0.1 mmol), in a mixture of THF/MeOH 1:1, imidazole-2-carbaldehyde (49 μL , 0.40 mmol) and then, 3-phenylpropyl isocyanide (68 μL , 0.40 mmol) and TMSN_3 (53 μL , 0.40 mmol) were added to carry out the on solid phase Ugi-azide-4CR as described in the general procedure. Compound **19** (23 mg, 60 %) was obtained as a light brown solid. $R_t = 10.3/10.5$ min. A mixture of diastereomers in a 4.7:1 ratio was observed by NMR. ^1H NMR (400 MHz, CD_3OD): $\delta = 0.89$ (d, 3H, $J = 6.8$ Hz, CH_3); 0.92 (d, 3H, $J = 6.8$ Hz, CH_3); 1.93 – 2.13 (m, 2H); 2.25 – 2.38 (m, 2H); 2.70 – 2.81 (m, 2H); 3.06 (d, 1H, $J = 4.3$ Hz, CH); 4.49 – 4.62 (m, 2H); 5.81 (s, 1H); 7.09 - 7.26 (m, 5H, Ar); 7.53 (s, 2H, Ar). ^{13}C NMR (100 MHz, CDCl_3): $\delta = 18.4, 19.6$ (CH_3); 32.0 (CH_2); 32.9 (CH); 33.6, 54.8 (CH_2); 65.1 (CH_3); 65.9, 121.2, 121.6, 127.4, 129.3, 129.6 (CH), 141.7, 145.1, 153.3 (C); 176.3 (C=O). HRMS: $m/z = 384.2136$ [$\text{M} + \text{H}$] $^+$ (calculated for $\text{C}_{19}\text{H}_{26}\text{N}_7\text{O}_2$: 384.2148); 767.4206 [$2\text{M} + \text{H}$] $^+$ (calculated for $\text{C}_{38}\text{H}_{51}\text{N}_{14}\text{O}_4$: 767.4218).

Compound 20. To L-Phe-loaded Wang resin (ca. 0.1 mmol), in a mixture of THF/MeOH 1:1, 2-furaldehyde (33 μL , 0.40 mmol) and then, cyclohexyl isocyanide (50 μL , 0.40 mmol) and TMSN_3 (53 μL , 0.40 mmol) were added to carry out the on solid phase Ugi-azide-4CR as described in the general procedure. Compound **20** (26 mg, 66 %) was obtained as a light brown solid. $R_t = 15.6$ min. A mixture of diastereomers in a 1:1 ratio was observed by NMR. ^1H NMR (400 MHz, CD_3OD): $\delta = 1.15 - 1.58$ (m, 4H); 1.63 – 1.93 (m, 7H); 2.87 (dd, 1H, $J = 13.7/ 8.7$ Hz, CH_2); 3.14 (dd, 1H, $J = 13.7/ 4.7$ Hz, CH_2); 3.55 (dd, 1H, $J = 8.7/ 4.7$ Hz, CH); 4.41 (tt, 1H, $J = 11.6/ 3.8$ Hz); 5.54 (s, 1H); 6.23 (d, 1H, $J = 3.2$ Hz, Ar); 6.38 (dd, 1H, $J = 3.2/ 1.9$ Hz, Ar); 7.18 – 7.35 (m, 5H, Ar); 7.43 (d, $J = 1.8$ Hz, 1H, Ar). ^{13}C NMR (100 MHz, CD_3OD): $\delta = 26.1, 26.3, 33.9, 40.1$ (CH_2); 51.1, 59.5, 61.6, 109.4; 110.4, 111.6, 129.5, 130.4 (CH); 139.0 (C); 144.6 (CH), 151.0, 154.6 (C); 176.4 (C=O). HRMS:

$m/z = 396.2021$ $[M+H]^+$ (calculated for $C_{21}H_{26}N_5O_3$: 396.2036); 791.3973 $[2M+H]^+$ (calculated for $C_{42}H_{51}N_{10}O_6$: 791.3993).

Compound 21. To a L-Phe-loaded Wang resin (ca. 0.1 mmol), in a mixture of THF/MeOH 1:1, 2-furaldehyde (33 μ L, 0.40 mmol), and then, benzyl isocyanide (50 μ L, 0.40 mmol) and TMSN₃ (53 μ L, 0.40 mmol) were added to carry out the on solid phase Ugi-azide-4CR as described in the general procedure. Compound **21** (30 mg, 75 %) was obtained as a light brown syrup. $R_t = 15.2$ min. A mixture of diastereomers in a 1:1 ratio was observed by NMR. ¹H NMR (400 MHz, CD₃OD): $\delta = 2.71$ (dd, 1H, $J = 13.6/8.9$ Hz, CH₂); 2.93 (dd, 1H, $J = 13.6/4.7$ Hz, CH₂); 3.42 (dd, 1H, $J = 8.9/4.7$ Hz, CH); 4.83 (d, 1H, $J = 15.7$ Hz); 5.32 (d, 1H, $J = 15.7$ Hz); 5.44 (s, 1H); 6.06 (d, 1H, $J = 3.3$ Hz, Ar); 6.18 (dd, 1H, $J = 3.3/1.9$ Hz, Ar); 6.76 – 6.80 (m, 1H, Ar); 6.99 – 7.24 (m, 10H, Ar). ¹³C NMR (100 MHz, CD₃OD): $\delta = 40.0, 51.7$ (CH₂); 51.8, 61.8, 109.7; 109.9, 127.7, 128.9, 129.3, 129.5, 129.8, 130.3 (CH); 135.3, 138.6 (C); 144.2 (CH), 150.6, 155.4 (C); 176.3 (C=O). HRMS: $m/z = 404.1708$ $[M+H]^+$ (calculated for $C_{22}H_{22}N_5O_3$: 404.1723); 807.3346 $[2M+H]^+$ (calculated for $C_{44}H_{43}N_{10}O_6$: 808.3367).

4.2. Biology

4.2.1. M1-alanyl-aminopeptidases from *Escherichia coli* and porcine microsomes (pmAPN)

Recombinant ePepN (rePepN) was overexpressed in *E. coli* and purified in an Ionic Exchange step as was previously described [75]. Porcine APN enzyme was used as a model of the human APN, since both share a high sequence similarity and show very similar kinetic properties [76]. This enzyme associated to the microsomes of the porcine kidney cortex was used [61] with the aim to study the selectivity of the selected inhibitors.

4.2.2. Murine myeloma P3X63Ag cells

Murine myeloma P3X63Ag was obtained from American Type Culture Collection (ATCC). Cells were cultured in DMEM-F12 (Gibco-BR, Paisley, UK), supplemented with 10% heat inactivated fetal calf serum (FCS) (Invitrogen, USA), 2 mM L-glutamine, 25 mM HEPES, 100 U/mL penicillin, 100 mg/mL streptomycin, and maintained at 37°C with 5 % CO₂.

4.2.3. Aminopeptidase activity assay for recombinant ePepN and pmAPN

The AP enzymatic activity (EA) was determined by a continuous kinetic method [77]. The chromogenic substrate Leu-pNA (Bachem, Sweden) 75 μM was used (~ 1 apparent Michaelis-Menten's constant (K_{Mapp}); dissolved in DMSO; 2 μL for the microplate assay and 10 μL for the cuvette assay) and the increase of the absorbance at 405 nm (due to the liberation of the pNA chromogen) was registered in function of time during 3 min, realizing measurements each 15 sec. The determinations were realized at 25°C, as in 96-well microplates (200 μL final volume), using a microplate spectrophotometer (Multiscan FC, Thermo Scientific, EUA), as in a cuvette of 1 cm of path length (1 mL final volume), using a kinetic spectrophotometer (UV-1800 Shimadzu, UV Spectrophotometer, Japan). The buffer 50 mM Tris-HCl pH 8.0 was used, as well as volumes of ePepN or pmAPN linearly related with the initial velocities (v_0). The final DMSO concentration in the assays was not higher than 2 % (v/v). Only the linear portions of the progress curves, corresponding to substrate consumption lower than 5%, were used to measure the reaction rates. The slopes with $R^2 < 0.98$ were not considered. The slope values of the reaction progress curves ($\Delta Abs/\Delta t$) were taken as values of v_0 . The assays were performed in triplicate.

4.2.4. Aminopeptidase activity inhibition assays for ePepN and pmAPN

The recombinant ePepN or pmAPN enzymes were pre-incubated with 10 μ L (for the cuvette assay) or 2 μ L (for the microplate assay) of bestatin or the compounds (dissolved in DMSO), at 25°C for 15 min. Subsequently, the substrate Leu-pNA at 75 μ M ($\sim 1 K_{Mapp}$) was added and the assays of AP activity were performed. The control was prepared by the pre-incubation of the enzyme with the same volume of DMSO in the previous conditions. The residual activity (v_i/v_0) was defined as the ratio between the reaction rate in the presence of the compound and the reaction rate corresponding to the control.

4.2.5. Dose-response studies for the inhibition of the ePepN and pmAPN enzymes

The inhibition assays of the ePepN's EA were performed as was previously described, with the 21 TPMs. Compounds **2**, **4** and **11** were also evaluated in the pmAPN inhibition assays. In all cases, different concentrations of each compound were used (prepared in DMSO by double serial dilutions) spanning the range 0.781–100 μ mol/L (concentrations in the assay). When the IC_{50} value was not reached in this range, lower or higher inhibitor concentrations were tested. The IC_{50} values were calculated by the nonlinear fit of the logistic function to the experimental data, using OriginPro 8 SR0 software (version 8.0724 (B724); OriginLab Corporation [<http://www.OriginLab.com>]) with default parameters. The logistic function is: $y = 1 / (1 + [I] / IC_{50})$, where y : residual AP activity, and $[I]$: inhibitor concentration in the assay [78]. All assays were performed at least in triplicate.

4.2.6. Determination of the time necessary to reach the inhibition equilibrium

Inhibition assays with ePepN and TPM **11** were performed with pre-incubation of the enzyme with the inhibitor during 5, 10, 15, 30 and 45 min.

4.2.7. Determination of the inhibition mode

Assays of AP EA with ePepN were performed as previously described, in the presence of the compound **11** at the concentrations 0, 1.56, 3.125 and 6.25 μM . For each inhibitor concentration, after pre-incubation for 15 min, the substrate Leu-*p*NA was added at different concentrations, spanning the range 18.75-1200 μM in the assay. In the absence of inhibitor, the enzyme was pre-incubated with the same DMSO volume. The experimental data were transformed and the Lineweaver-Burk double reciprocal plots were constructed. The equation is: $1/v_0 = (K_{Mapp} / v_{maxapp}) (1/[S]_0) + 1/v_{maxapp}$, where v_{maxapp} : apparent maximal rate of the enzymatic reaction, and $[S]_0$: initial substrate concentration in the assay [78]. The transformed experimental data were analyzed by a simple linear fitting using the software Microsoft Office Excel 2007TM (Microsoft Corporation; EUA; [<https://www.microsoft.com/>]). The inhibition type was determined graphically from the lines of the double reciprocal plots [78].

4.2.8. Structural and molecular docking studies

In silico studies were focused on the most potent compound of the studied series, *i.e.* TPM **11**. The putative binding modes of both TPM **11** diastereomers were predicted by combining structural analysis and docking simulations. Two-dimensional structures of compounds were used to build 3D models from the corresponding SDF files. Because inhibitors were evaluated as diastereomeric mixtures, we considered the two possible configurations of TPM **11** at position R^2 using ChemAxon software [79], while the configuration of the amino acid residue R^1 is always (*S*). For clarity, we named isomers according to the structure around the asymmetric carbon bonded to R^2 (Fig. S6). The 3D

structures of both TPM **11** diastereomers were minimized in Avogadro using the MMFF94 force field [80]. Protonation states of protein residues were calculated using PDB2PQR [81]. We took care that histidine residues interacting with Zn atom were properly protonated. PDBQT files were generated with AutoDockTools [82]. Molecular docking simulations were conducted with the Autodock4_{Zn} force field [83]. The receptor coordinates were chosen based on the analysis of all the available non-redundant 3D X-ray structures of ePepN retrieved from the Protein Data Bank repository (<http://www.rcsb.org/pdb>).

4.2.9. Molecular dynamic simulations

In order to assess the stability of the predicted complexes, MD simulations were performed. Predicted structures were used as starting points for MD simulations of 30 ns, using the GROMACS (version 4.6.5) software package [84], periodic boundary conditions (PBC), and the Amber99sb force field [85]. Protonation states of protein residues were calculated as described above. Ligand parameters were generated from the general Amber force field (GAFF) [86], and charges were calculated using AM1-BCC, a semi-empirical approximation available in the Antechamber program [87,88].

All systems were neutralized (Na^+/Cl^-) and solvated with explicit water molecules, which were modelled by the TIP3P [89] parameter set, in a rhombic dodecahedron box. The distance between the protein-ligand complexes and the edge of the box were set to 10 Å. The LINCS algorithm was used to constrain all the covalent bonds in non-water molecules [90], while the SETTLE algorithm was used to constrain bond lengths and angles in water molecules [91].

To avoid Zn^{2+} ion unbinding from the active site and/or incorrect pseudovalence bond formation (due to the use of a classical force field), a 10 kcal/(mol \AA^2) harmonic constraint was applied on the Zn^{2+} ion for ensuring a correct ligation state. A similar constraint was applied to heavy atoms of both, the protein and the ligand, in order to prevent unbinding processes during system's equilibration and thermalization stages [92].

Energy minimization was carried out using a steepest descent algorithm followed by the conjugate gradient method. Then, systems were gradually heated for 300 ps to reach the experimentally reported assay temperature. The Leapfrog scheme [93], with an integration time step of 2 fs, was employed to integrate the equations of motion. The temperature was controlled using a weak coupling to a bath with a time constant of 0.1 ps [94]. For pressure control, a Berendsen coupling algorithm with a time constant of 1.0 ps was employed [94]. Initial velocities were randomly generated from a Maxwell distribution at 50 K, in accordance with the atomic masses.

In order to preserve the coordination geometry throughout the production run, a 10 kcal/(mol \AA^2) harmonic constraint was applied on the Zn^{2+} ion, as well as the heavy atoms of the residues His²⁹⁷, His³⁰¹ and Glu³²⁰ coordinating the Zn^{2+} ion. Furthermore, a small (0.5 kcal/(mol \AA^2)) harmonic constraint was applied on the C α atoms of the residues beyond the active site to avoid undesirable artefacts due to applied constraints for preserving coordination geometry. The heavy atoms of the ligands and those of the residues belonging to the active site were kept unrestrained [92].

The Leapfrog scheme [93], with an integration time step of 2 fs, was employed to integrate the equations of motion. The temperature was controlled using a weak coupling to a bath with a time constant of 2.0 ps. For pressure control, a Parrinello-Rahman [95] coupling

algorithm with a time constant of 5.0 ps was employed. Long-range electrostatic interactions were handled by Particle Mesh Ewald (PME) summation [71,96]. The van der Waals interactions were modelled by Lennard-Jones (6-12) potential [84]. As GROMACS is not straightforward to obtain long-range electrostatic contributions from the PME algorithm, these were recalculated using the Reaction Field zero algorithm throughout the generated trajectory [84]. All ligands were solvated in a rhombic dodecahedron box with the same size as the one generated for its respective protein-ligand complex. Finally, 5 ns simulations were run using the above protocol.

4.2.10. Free energy calculations

In order to validate docking results, we used the Linear Interaction Energy approach proposed by Miranda *et al.* [65,97] (coined LIE-D) to predict binding free energies. The LIE-D formula takes into account the intra-ligand electrostatic interactions as suggested by Almlöf *et al.* [98] and takes the form of equation 1:

$$\Delta G^{bind} = \beta_{FEP}(\Delta\langle V_{i-s}^{el} \rangle + \Delta\langle V_{i-l}^{el} \rangle) + \alpha\Delta\langle V_{i-s}^{vdW} \rangle + \gamma \quad (1)$$

where ΔG^{bind} is the predicted binding free energy, $\Delta\langle V_{i-s}^{el} \rangle + \Delta\langle V_{i-l}^{el} \rangle$ and $\Delta\langle V_{i-s}^{vdW} \rangle$ denotes the change of both intra-ligand electrostatic and van der Waals interactions when it is transferred from solution (free state) into the solvated receptor binding site (bound state).

We calculated a β_{FEP} specific values for each ligand using the parameterization model E proposed by Almlöf *et al.* [98] and α value was set in 0.18. We calculated γ using the linear correlation between D parameter and γ (equation 2) [65]:

$$\gamma = f x D + g \text{ [kcal/mol]} \quad (2)$$

where f and g are the slope (-0.95) and intercept (-2.06), respectively.

The D parameter encompasses the balance (difference) between electrostatic (polar) and van der Waals (non-polar) energies in protein-ligand complexes (equation 3) [65]:

$$D = \beta (\Delta \langle V_{i-s}^{el} \rangle + \Delta \langle V_{i-l}^{el} \rangle) - \alpha \Delta \langle V_{i-s}^{vdW} \rangle \text{ [kcal/mol]} \quad (3)$$

4.2.11. Activity landscape modelling. Similarity/activity cliffs analysis

Similarity/activity cliffs analysis was performed with DataWarrior program [68]. Similarity criterion for arranging molecules on the 2D-map was based on the default *FragFp* descriptor. A similarity threshold was set to 85 % for establishing similarity relationships. In addition to the similarity analysis, the so-called Structure-Activity Landscape Index (SALI) was calculated for all pairs of similar molecules. The SALI value is a measure of how much activity is gained (or lost) with a relatively small change in structure and, it was calculated as follows [68,72]:

$$SALI = \frac{|pIC_{50}^1 - pIC_{50}^2|}{1 - s} \quad (4)$$

being s , the structural similarity between the molecules and pIC_{50}^1/pIC_{50}^2 the activities of two neighbors. SALI was calculated for every compounds identified as neighbors.

4.2.12. Inhibition assay for the *in vitro* growth of *E. coli* BL21

Cultures of *E. coli* BL21 were prepared by inoculation with the 1 % volume from an overnight culture, in 200 μ L-aliquots of LB medium in 96-well plates. The cultures were exposed to eight concentrations of compounds: bestatin (positive control of ePepN inhibition), **2**, **4**, **11** and **16** (negative control of ePepN inhibition), prepared by double serial dilutions in DMSO and spanning the range 0.781-100 μ M (assay concentrations). In addition, were prepared cultures non-exposed to neither compound, other treated with

DMSO (positive control of growth), and other exposed to 200 $\mu\text{g}/\text{mL}$ ampicillin antibiotic (negative control of growth). Also was used non-inoculated medium as blank and control of contamination. Four replicates by condition were tested. The cultures were incubated for 20 h at 37°C, and the absorbance at 595 nm was assessed in a microplate spectrophotometer at 0, 3, 6 and 20 h. The temperature was increased at 42°C at 6 h of culture. Finally, the dose-response curves were constructed, normalizing the DO values as regards the DMSO control, taken as 100 % of growth.

4.2.13. Haemolytic activity

The cytotoxic effect of the compounds on erythrocytes was evaluated by the haemolysis according to [99]. In brief, erythrocyte suspensions were prepared using fresh human red blood cells, washed and resuspended in physiological buffer solution (PBS: 145 mM NaCl, 10 mM Tris-HCl pH 7.4). The concentration of the standard cellular suspension was adjusted by addition of PBS to obtain an approximate absorbance of 0.7 at 540 nm when one mL of the suspension of cells was totally lysed with 14 mL Na_2CO_3 (0.1 %). The haemolytic activity (HA) was evaluated by the amount of haemoglobin remaining in the supernatant after centrifugation after 3 h, 6 h and 20 h of incubation with the compounds. Cells without treatment were used as control and cells treated with DMSO (1 %) were used to verify the effect of DMSO.

4.2.14. MTT assay

Viable cells were quantified by the MTT colorimetric assay, which measures tetrazolium dye 3-(4,5-dimethylthiazol-2-yl)-2,5-diphenyltetrazolium bromide reduction by mitochondrial enzymes [74]. Briefly, P3X63Ag cells were plated with serum-free

DMEMF12 medium and treated with different concentrations of compounds for 3 h, 6 h and 20 h. After washing with PBS, MTT was added to the cells for three hours; next, the crystals were dissolved with DMSO and the absorbance was measured in an ELISA reader (Organon Teknika, Salsburg, Austria) at 450 nm with the 620 nm as reference. Cells without treatment were used as control. Cellular viability (%) was calculated from the following equation:

$$\text{Cellular viability (\%)} = 100 \times A_t / A_c$$

where A_t is the absorbance of treated cells and A_c is the absorbance of non-treated cells (control cells).

4.2.15. Statistical analyses

Normal distribution and homogeneity of variances of the experimental data were verified by the Kolmogorov-Smirnov and the Bartlett test, respectively [100]. Afterward, an analysis of variance of simple classification was carried out. The means were compared by the Tukey HSD test [101]. A level of signification of 0.05 was used. To perform these analyses, the software Statistica (version 8.0; StatSoft Inc. [<http://www.statsoft.com>]) was used.

Declaration of interest: none

Acknowledgments

This work was supported by the International Foundation for Sciences (grant F/4730-2), by the project assigned to J. González-Bacerio and associated to the Cuban National Program of Basic Science, and by the BMBF project (CUB17WTZ-068, Germany). Y. Mendez and

A. V. Vasco are grateful to DAAD for PhD scholarships and D. G. Rivera to the Alexander von Humboldt Foundation for an Experienced Researcher fellowship.

Appendix A. Supplementary data

^1H and ^{13}C NMR spectra and analytical HPLC traces of pure compounds. Details of the biological evaluation and docking simulation.

References

- [1] E.D. Brown, G.D. Wright, Antibacterial drug discovery in the resistance era, *Nature* 529 (2016) 336–343.
- [2] A. Addlagatta, L. Gay, B.W. Matthews, Structure of aminopeptidase N from *Escherichia coli* suggests a compartmentalized, gated active site, *Proc. Natl. Acad. Sci. U.S.A.* 103 (2006) 13339–13344.
- [3] N. Drinkwater, J. Lee, W. Yang, T.R. Malcolm, S. McGowan, M1 aminopeptidases as drug targets: broad applications or therapeutic niche?, *FEBS J.* 12 (2017) 3218–3221.
- [4] M.J. Kuehn, N.C. Kesty, Bacterial outer membrane vesicles and the host – pathogen interaction, *Genes Dev.* 19 (2005) 2645–2655.
- [5] D. Chandu, D. Nandi, PepN is the major aminopeptidase in *Escherichia coli*: Insights on substrate specificity and role during sodium-salicylate-induced stress, *Microbiology* 149 (2003) 3437–3447.
- [6] A. Mucha, M. Drag, J.P. Dalton, P. Kafarski, Metallo-aminopeptidase inhibitors, *Biochimie* 92 (2010) 1509–1529.

- [7] N.D. Rawlings, A.J. Barrett, R. Finn, Twenty years of the MEROPS database of proteolytic enzymes, their substrates and inhibitors, *Nucleic Acids Res.* 44 (2016) D343–D350.
- [8] M.B. Harbut, G. Velmourougane, G. Reiss, R. Chandramohanadas, D.C. Greenbaum, Development of bestatin-based activity-based probes for metallo-aminopeptidases, *Bioorg. Med. Chem. Lett.* 18 (2008) 5932–5936.
- [9] E. Cunningham, M. Drag, P. Kafarski, A. Bell, Chemical target validation studies of aminopeptidase in malaria parasites using α -aminoalkylphosphonate and phosphonopeptide inhibitors, *Antimicrob. Agents Chemother.* 52 (2008) 3221–3228.
- [10] D. Chandu, A. Kumar, D. Nandi, PepN, the major Suc-LLVY-AMC-hydrolyzing enzyme in *Escherichia coli*, displays functional similarity with downstream processing enzymes in archaea and eukarya, *J. Biol. Chem.* 278 (2003) 5548–5556.
- [11] S. Gharbi, A. Belaich, M. Murgier, A. Lazdunski, Multiple controls exerted on *in vivo* expression of the pepN gene in *Escherichia coli*: Studies with pepN-lacZ operon and protein fusion strains, *J. Bacteriol.* 163 (1985) 1191–1195.
- [12] A. Kumar, M. Bhosale, S. Reddy, N. Srinivasan, D. Nandi, Importance of non-conserved distal carboxyl terminal amino acids in two peptidases belonging to the M1 family: *Thermoplasma acidophilum* Tricorn interacting factor F2 and *Escherichia coli* Peptidase N, *Biochimie* 91 (2009) 1145–1155.
- [13] M. Bhosale, A. Kumar, M. Das, C. Bhaskarla, V. Agarwal, Catalytic activity of Peptidase N is required for adaptation of *Escherichia coli* to nutritional downshift

and high temperature stress, *Microbiol. Res.* 168 (2013) 56–64.

- [14] T. Kazakov, G. Vondenhoff, K. Datsenko, M. Novikova, A. Metlitskaya, B. Wanner, K. Severinov, *Escherichia coli* peptidase A, B, or N can process translation inhibitor microcin C, *J. Bacteriol.* 190 (2008) 2607–2610.
- [15] J. González-Bacero, S. El C. Maluf, Y. Méndez, I. Pascual, I. Florent, P.M.S. Melo, A. Budu, J.C. Ferreira, E. Moreno, A.K. Carmona, D.G. Rivera, M. Alonso, M.L. Gazarini, KBE009: An antimalarial bestatin-like inhibitor of the *Plasmodium falciparum* M1 aminopeptidase discovered in an Ugi multicomponent reaction-derived peptidomimetic library, *Bioorg. Med. Chem.* 25 (2017) 4628–4636.
- [16] Y. Méndez, K. Pérez-Labrada, J. González-Bacero, G. Valdés, M. A. Chávez, J. Osuna, J. L. Charli, I. Pascual, D. G. Rivera, Combinatorial Multicomponent Access to Natural Products-Inspired Peptidomimetics: Discovery of Selective Inhibitors of Microbial Metallo-Aminopeptidases, *Chem. Med Chem.* 9 (2014) 2351-2359.
- [17] L.V. Myznikov, A. Hrabalek, G.I. Koldobskii, Drugs in the tetrazole series, *Chem. Heterocycle Compd.* 43 (2007) 1–9.
- [18] P.A. Cano, A. Islas-Jácome, J. González-Marrero, L. Yépez-Mulia, F. Calzada, R. Gámez-Montaño, Synthesis of 3-tetrazolylmethyl-4H -chromen-4-ones via Ugi-azide and biological evaluation against *Entamoeba histolytica*, *Giardia lamblia* and *Trichomona vaginalis*, *Bioorg. Med. Chem.* 22 (2014) 1370–1376.
- [19] P.A. Cano, A. Islas-Jácome, Á. Rangel-Serrano, F. Anaya-Velázquez, F. Padilla-Vaca, E. Trujillo-Esquivel, P. Ponce-Noyola, A. Martínez-Richa, R. Gámez-Montaño, *In Vitro* studies of chromone-tetrazoles against pathogenic protozoa,

- bacteria, and fungi, *Molecules* 20 (2015) 12436–12449.
- [20] G. Aromí, L.A. Barrios, O. Roubeau, P. Gamez, Triazoles and tetrazoles: Prime ligands to generate remarkable coordination materials, *Coord. Chem. Rev.* 255 (2011) 485–546.
- [21] I. Ugi, C. Steinbrückner, Isonitrile, II. Reaktion von isonitrilen mit carbonylverbindungen, aminen und stickstoffwasserstoffsäure, *Chem. Ber.* 94 (1961) 734–742.
- [22] A. Maleki, A. Sarvary, Synthesis of tetrazoles via isocyanide-based reactions, *RSC Adv.* 5 (2015) 60938–60955.
- [23] S. Ramezani, S. Balalaie, F. Rominger, N.S. Alavijeh, H. Reza, Facile, efficient and diastereoselective synthesis of α -hydrazine tetrazoles through a novel one-pot four-component reaction, *Tetrahedron* 69 (2013) 10718–10723.
- [24] A. Nikbakht, S. Ramezani, S. Balalaie, F. Rominger, Efficient and stereoselective synthesis of α -hydrazino tetrazoles through a pseudo five-component domino reaction, *Tetrahedron* 71 (2015) 6790–6795.
- [25] N.S. Alavijeh, R. Zadmand, S. Ramezani, S. Balalaie, M.S. Alavijeh, F. Rominger, Efficient synthesis of lower rim α -hydrazino tetrazolocalix[4]arenes via an Ugi-azide multicomponent reaction, *New J. Chem.* 39 (2015) 6578–6584.
- [26] P. Patil, J. Zhang, K. Kurpiewska, J. Kalinowska-Łuszczak, A. Dömling, Hydrazine in the Ugi tetrazole reaction, *Synthesis* 48 (2016) 1122–1130.
- [27] A.F.S. Barreto, V.A. dos Santos, C.K.Z. Andrade, Consecutive hydrazino-Ugi-azide

- reactions: synthesis of acylhydrazines bearing 1,5-disubstituted tetrazoles, *Beilstein J. Org. Chem.* 13 (2017) 2596–2602.
- [28] Y. Wang, P. Patil, K. Kurpiewska, J. Kalinowska-Tluscik, A. Dömling, Two cycles with one catch: Hydrazine in Ugi 4-CR and its postcyclizations, *ACS Comb. Sci.* 19 (2017) 193–198.
- [29] L.E. Cárdenas-Galindo, A. Islas-Jácome, N.V. Álvarez-Rodríguez, E. Kaim, R. Gámez-Montaño, Synthesis of 2-tetrazolylmethyl-2,3,4,9-tetrahydro-1H- β -carbolines by a one-pot Ugi-azide/Pictet–Spengler process, *Synthesis* 46 (2013) 49–56.
- [30] M. Ghandi, S. Rahimi, N. Zarezadeh, Synthesis of novel tetrazole containing quinoline and 2,3,4,9-tetrahydro-1H- β -carboline derivatives, *J. Heterocycl. Chem.* 54 (2017) 102–109.
- [31] D. G. Rivera, K. Pérez-Labrada, L. Lambert, S. Dörner, B. Westermann, L. A. Wessjohann, Carbohydrate–steroid conjugation by Ugi reaction: one-pot synthesis of triple sugar/pseudo-peptide/spirostane hybrids. *Carbohydr. Res.* 359 (2012) 102–110.
- [32] P. Purohit, A.K. Pandey, D. Singh, P.S. Chouhan, K. Ramalingam, M. Shukla, N. Goyal, J. Lal, P.M.S. Chauhan, An insight into tetrahydro- β -carboline-tetrazole hybrids: synthesis and bioevaluation as potent antileishmanial agents, *MedChemComm* 8 (2017) 1824–1834.
- [33] T. Nixey, M. Kelly, C. Hulme, The one-pot solution phase preparation of fused tetrazole-ketopiperazines, *Tetrahedron Lett.* 41 (2000) 8729–8733.

- [34] M. Ghandi, F. Sherafat, Expedient access to novel bis-tetrazolopiperazines via Ugi-azide reactions, *J. Heterocycl. Chem.* 54 (2017) 1396–1403.
- [35] M. Ghandi, S. Salahi, A. Taheri, A. Abbasi, One-pot synthesis of novel 1-(1*H*-tetrazol-5-yl)-1,2,3,4-tetrahydropyrrolo[1,2-*a*]pyrazine derivatives via an Ugi-azide 4CR process, *Mol. Divers.* 22 (2018) 291–303.
- [36] P. Patil, R. Madhavachary, K. Kurpiewska, J. Kalinowska-Tluscik, A. Dömling, De novo assembly of highly substituted morpholines and piperazines, *Org. Lett.* 19 (2017) 642–645.
- [37] S.G. Yerande, K.M. Newase, B. Singh, A. Boltjes, A. Dömling, Application of cyclic ketones in MCR:Ugi/amide coupling based synthesis of fused tetrazolo[1,5-*a*][1,4]benzodiazepines, *Tetrahedron Lett.* 55 (2014) 3263–3266.
- [38] F. Medda, G. Martinez-Ariza, C. Hulme, A facile and concise route toward the synthesis of novel imidazo-tetrazolodiazepinones via post-condensation modifications of the Ugi-azide adduct, *Tetrahedron Lett.* 56 (2015) 5295–5298.
- [39] B.V.S. Reddy, K. Kota, B.M. Rao, B. Sridhar, K. Mukkanti, Four-component, five-centered, one-pot synthesis of 1-(1*H*-tetrazol-5-yl)-2,3,4,9-tetrahydro-1*H*-pyrido[3,4-*b*]indole derivatives, *Tetrahedron Lett.* 57 (2016) 4529–4532.
- [40] A. Rentería-Gómez, A. Islas-Jácome, A.E. Cruz-Jiménez, J.C. Manzano-Velázquez, S. Rojas-Lima, J.O.C. Jiménez-Halla, R. Gámez-Montaña, Synthesis of 2-tetrazolylmethyl-isoindolin-1-ones via a one-pot Ugi-azide/(*N*-acylation/*exo*-Diels-Alder)/dehydration process, *ACS Omega* 1 (2016) 943–951.

- [41] V. Estévez, L. Kloeters, N. Kwietniewska, E. Vicente-García, E. Ruijter, R.V.A. Orru, Ugi-type reactions of spirocyclic indolenines as a platform for compound library generation, *Synlett.* 28 (2017) 376–380.
- [42] G.P. Liao, E.M.M. Abdelraheem, C.G. Neochoritis, K. Kurpiewska, J. Kalinowska-Tluscik, D.C. McGowan, A. Dömling, Versatile multicomponent reaction macrocycle synthesis using α -isocyano- ω -carboxylic acids, *Org. Lett.* 17 (2015) 4980–4983.
- [43] E.M.M. Abdelraheem, M.P. De Haan, P. Patil, K. Kurpiewska, J. Kalinowska-Tluscik, S. Shaabani, A. Dömling, Concise synthesis of tetrazole macrocycle, *Org. Lett.* 19 (2017) 5078–5081.
- [44] P. Patil, B. Mishra, G. Sheombarsing, K. Kurpiewska, J. Kalinowska-Tluscik, A. Dömling, Library-to-library synthesis of highly substituted α -aminomethyl tetrazoles via Ugi reaction, *ACS Comb. Sci.* 20 (2018) 70–74.
- [45] R. Madhavachary, Q. Wang, A. Dömling, With unprotected amino acids to tetrazolo peptidomimetics, *Chem. Commun.* 53 (2017) 8549–8552.
- [46] S.G. Pharande, A. Rosa, C. Escobosa, R. Gámez-Montaña, Endogenous water-triggered and ultrasound accelerated synthesis of 1,5-disubstituted tetrazoles via a solvent and catalyst-free Ugi-azide reaction, *Green Chem.* 19 (2017) 1259–1262.
- [47] D.P. Zarezin, V.N. Khrustalev, V.G. Nenajdenko, Diastereoselectivity of azido-Ugi reaction with secondary amines. Stereoselective synthesis of tetrazole derivatives, *J. Org. Chem.* 82 (2017) 6100–6107.

- [48] F. Constabel, I. Ugi, Repetitive Ugi reactions, *Tetrahedron* 57 (2001) 5785–5789.
- [49] J.J. Chen, A. Golebiowski, S.R. Klopfenstein, L. West, The universal Rink-isonitrile resin: applications in Ugi reactions, *Tetrahedron Lett.* 43 (2002) 4083–4085.
- [50] W.L. Scott, M.J. O'Donnell, Distributed drug discovery, Part 1: Linking academia and combinatorial chemistry to find drug leads for developing world diseases, *J. Comb. Chem.* 11 (2009) 3–13.
- [51] W.L. Scott, R.E. Denton, K.A. Marrs, J.D. Durrant, J.G. Samaritoni, M.M. Abraham, S.P. Brown, J.M. Carnahan, L.G. Fischer, C.E. Glos, P.J. Sempsrott, M.J.O. Donnell, Distributed drug discovery: Advancing chemical education through contextualized combinatorial solid-phase organic laboratories, *J. Chem. Educ.* 92 (2015) 819–826.
- [52] A. Addlagatta, L. Gay, B.W. Matthews, Structural basis for the unusual specificity of *Escherichia coli* aminopeptidase N, *Biochemistry* 47(2008) 5301–5311.
- [53] F.E. Morales, H.E. Garay, D.F. Muñoz, Y.E. Augusto, A.J. Otero-González, O.R. Acosta, D.G. Rivera, Aminocatalysis-mediated on-resin Ugi reactions: Application in the solid-phase synthesis of *N*-substituted and tetrazolo lipopeptides and peptidosteroids, *Org. Lett.* 17 (2015) 2728–2731.
- [54] M. Morejón, A. Laub, B. Westermann, D.G. Rivera, L.A. Wessjohann, Solution- and Solid-Phase Macrocyclization of Peptides by the Ugi–Smiles Multicomponent Reaction: Synthesis of *N*-Aryl-Bridged Cyclic Lipopeptides, *Org. Lett.* 18 (2016) 4096–4099.
- [55] A.R. Puentes, M.C. Morejón, D.G. Rivera, L.A. Wessjohann, Peptide

- Macrocyclization Assisted by Traceless Turn Inducers Derived from Ugi Peptide Ligation with Cleavable and Resin-Linked Amines, *Org. Lett.* 19 (2017) 4022–4025.
- [56] S. McGowan, C.J. Porter, J. Lowther, C.M. Stack, S.J. Golding, T.S. Skinner-Adams, K.R. Trenholme, F. Teuscher, S.M. Donnelly, J. Grembecka, A. Mucha, P. Kafarski, R. DeGori, A.M. Bucle, D.L. Gardiner, J.C. Whisstock, J.P. Dalton, Structural basis for the inhibition of the essential *Plasmodium falciparum* M1 neutral aminopeptidase, *Proc. Natl. Acad. Sci. U.S.A.* 106 (2009) 2537–2542.
- [57] L. Chen, Y-L. Lin, G. Peng, F. Li, Structural basis for multifunctional roles of mammalian aminopeptidase N, *Proc. Natl. Acad. Sci. U.S.A.* 109 (2012) 17966–17971.
- [58] A. Wong, D. Zhou, J. Rini, The X-ray crystal structure of human aminopeptidase N reveals a novel dimer and the basis for peptide processing, *J. Biol. Chem.* 287 (2012) 36804–36813.
- [59] K-W. Yang, F.C. Golich, T.K. Sigdel, M.W. Crowder, Phosphinate, sulfonate and sulfonamidate dipeptides as potential inhibitors of *Escherichia coli* aminopeptidase N, *Bioorg. Med. Chem. Lett.* 15 (2005) 5150–5153.
- [60] H. Chen, B. Roques, M. Fournie-Zaluski, Design of the first highly potent and selective aminopeptidase N (EC 3.4.11.2) inhibitor, *Bioorg. Med. Chem. Lett.* 9 (1999) 1511–1516.
- [61] A. Byzia, A. Szeffler, L. Kalinowski, M. Drag, Activity profiling of aminopeptidases in cell lysates using a fluorogenic substrate library, *Biochimie* 122 (2016) 31–37.
- [62] R. Rozenfeld, L. Muller, S. El Messari, C. Llorens-Cortes, The C-terminal domain of

- aminopeptidase A is an intramolecular chaperone required for the correct folding, cell surface expression, and activity of this monozinc aminopeptidase, *J. Biol. Chem.* 279 (2004) 43285–43295.
- [63] A. Albiston, S. YE, S. Chai, Membrane bound members of the M1 family: more than aminopeptidases, *Protein Pept.* 11 (2004) 491–500.
- [64] S. Dalal, D.R.T. Ragheb, F.D. Schubot, M. Klemba, A naturally variable residue in the S1 subsite of M1 family aminopeptidases modulates catalytic properties and promotes functional specialization, *J. Biol. Chem.* 288 (2013) 26004–26012.
- [65] W.E. Miranda, S.Y. Noskov, P.A. Valiente, Improving the LIE method for binding free energy calculations of protein–ligand complexes, *J. Chem. Inf. Model* 55 (2015) 1867–1877.
- [66] K. Ito, Y. Nakajima, Y. Onohara, M. Takeo, K. Nakashima, F. Matsubara, T. Ito, T. Yoshimoto, Crystal structure of aminopeptidase N (Proteobacteria alanyl aminopeptidase) from *Escherichia coli* and conformational change of methionine 260 involved in substrate recognition, *J. Biol. Chem.* 281 (2006) 33664–33676.
- [67] I. Pascual, P.A. Valiente, G. García, M.E. Valdés-Tresanco, Y. Arrebola, L. Díaz, L. Bounaadja, R.M. Uribe, M.C. Pacheco, I. Florent, J.-L. Charli, Discovery of novel non-competitive inhibitors of mammalian neutral M1 aminopeptidase (APN), *Biochimie* 142 (2017) 216–225.
- [68] T. Sander, OSIRIS DataWarrior, in, Idorsia Pharmaceuticals Ltd., 2018.
- [69] V. Martin, Progress with modeling activity landscapes in drug discovery, *Expert*

- Opin. Drug Discov. 13 (2018) 605–615.
- [70] E.S.R. Ehmki, M. Rarey, Exploring Structure-Activity Relationships with Three-Dimensional Matched Molecular Pairs-A Review, *ChemMedChem* 13 (2018) 482–489.
- [71] T. Darden, D. York, L. Pedersen, Particle Mesh Ewald: An $W \log(N)$ Method for Ewald Sums in Large Systems, *J. Chem. Phys.* 98 (1993) 10089–10093.
- [72] R. Guha, J. Van Drie, Structure-activity landscape index: Identifying and quantifying activity cliffs, *J. Chem. Inf. Model* 48 (2008) 646–658.
- [73] G. Li, K.D. Young, Indole production by the tryptophanase TnaA in *Escherichia coli* is determined by the amount of exogenous tryptophan, *Microbiology* 159 (2013) 402–410.
- [74] R.S. Gardner, A sensitive colorimetric assay for mitochondrial alpha glycerophosphate dehydrogenase, *Anal. Biochem.* 59 (1974) 272–276.
- [75] Y. Méndez, K. Pérez-Labrada, J. González-Bacero, G. Valdés, M.Á. de los Chávez, J. Osuna, J-L. Charli, I. Pascual, D.G. Rivera, Combinatorial multicomponent access to natural-products-inspired peptidomimetics: discovery of selective inhibitors of microbial metallo-aminopeptidases, *Chem. Med. Chem.* 9 (2014) 2351–2359.
- [76] X. Wang, L. Zhang, K. Yang, C. Zhang, J. Zhang, H. Fang, W. Xu, The effect of different species aminopeptidase N structure on the activity screening of aminopeptidase N inhibitor, *Biol. Pharm. Bull.* 33 (2010) 1658–1665.
- [77] S. Tiekou, N.M. Hooper, Inhibition of aminopeptidases N, A and W: A re-evaluation

of the action of bestatin and inhibitors of angiotensin converting enzyme, *Biochem. Pharmacol.* 44 (1992) 1725–1730.

- [78] R.A. Copeland, *Enzymes: A practical introduction to structure, mechanism, and data analysis*, Second Ed., Wiley-VCH, Inc., New York, 2000.
- [79] ChemAxon, Marvin 17.3.13.0, in, 2017.
- [80] M.D. Hanwell, D.E. Curtis, D.C. Lonie, T. Vandermeersch, E. Zurek, G.R. Hutchison, Avogadro: An advanced semantic chemical editor, visualization, and analysis platform, *J. Cheminform.* 4 (2012) 17
- [81] T.J. Dolinsky, J.E. Nielsen, J.A. McCammon, N.A. Baker, PDB2PQR: an automated pipeline for the setup of Poisson-Boltzmann electrostatics calculations, *Nucleic Acids Res.* 32(Web Server issue) (2004) W665–667.
- [82] M.F. Sanner, Python: a programming language for software integration and development, *J. Mol. Graphics Mod.* 17 (1999) 57–61.
- [83] D. Santos-Martins, S. Forli, M.J. Ramos, A.J. Olson, AutoDock4Zn: An Improved AutoDock Force Field for Small-Molecule Docking to Zinc Metalloproteins, *J. Chem. Inf. Model.* 54 (2014) 2371–2379.
- [84] D. van der Spoel, E. Lindahl, B. Hess, A.R. van Buuren, E. Apol, P.J. Meulenhoff, D.P. Tieleman, A.L.T.M. Sijbers, K.A. Feenstra, R. van Drunenand, H.J.C. Berendsen, *GROMACS User Manual*, Royal Institute of Technology and Uppsala University, Sweden, 2013.
- [85] V. Hornak, R. Abel, A. Okur, B. Strockbine, A. Roitberg, C. Simmerling,

Comparison of Multiple Amber Force Fields and Development of Improved Protein Backbone Parameters, *Proteins*, 65 (2006) 712–725.

- [86] J. Wang, R.M. Wolf, J.W. Caldwell, P.A. Kollman, D.A. Case, development and testing of a general amber force field, *J. Comp. Chem.* 25 (2004) 1157–1174.
- [87] A. Jakalian, B.L. Bush, D.B. Jack, C.I. Bayly, Fast, efficient generation of high-quality atomic charges, AM1-BCC model: I. Method, *J. Comput. Chem.* 21 (2000) 132–146.
- [88] A. Jakalian, D.B. Jack, C.I. Bayly, Fast, efficient generation of high-quality atomic charges. AM1-BCC model: II. Parameterization and Validation, *J. Comput. Chem.* 23 (2002) 1623–1641.
- [89] W. Jorgensen, J. Chandrasekhar, J. Madura, M. Klein, R.W. Impey, comparison of simple potential functions for simulating liquid water, *J. Chem. Phys.* 79 (1983) 926–935.
- [90] B. Hess, H. Bekker, H.J.C. Berendsen, J.G.E.M. Fraaije, LINCS: A linear constraint solver for molecular simulations, *J. Comput. Chem.* 18 (1997) 1463–1472.
- [91] S. Miyamoto, P.A. Kollman, Settle: an analytical version of the SHAKE and RATTLE algorithm for rigid water models, *J. Comput. Chem.* 13 (1992) 952–962.
- [92] T.J. Hou, W. Zhang, X.J. Xu, Binding Affinities for a Series of Selective Inhibitors of Gelatinase-A Using Molecular Dynamics with a Linear Interaction Energy Approach, *J. Phys. Chem. B*, 105 (2001) 5304–5315.
- [93] L. Verlet, Computer "experiments" on classical fluids I. Thermodynamical properties

- of Lennard-Jones molecules, *Phys. Rev.* 159 (1967) 98–103.
- [94] H.J.C. Berendsen, J.P.M. Postma, W.F. van Gunsteren, A. Dinola, J.R. Haak, Molecular dynamics with coupling to an external bath, *J. Chem. Phys.* 81 (1984) 3684–3690.
- [95] M. Parrinello, A. Rahman, Polymorphic transitions in single crystals: A new molecular dynamics method, *J. Appl. Phys.* 52 (1981) 7182–7190.
- [96] U. Essmann, L. Perera, M.L. Berkowitz, T. Darden, H. Lee, L.G. Pedersen, A smooth Particle Mesh Ewald method, *J. Chem. Phys.* 103 (1995) 8577–8592.
- [97] J. Åqvist, C. Medina, J. Samuelsson, A new method for predicting binding affinity in computer-aided drug design, *Prot. Eng.* 7 (1994) 385–391.
- [98] M. Almlöf, J. Carlsson, J. Åqvist, Improving the accuracy of the linear interaction energy method for solvation free energies, *J. Chem. Theory Comput.* 3 (2007) 2162–2175.
- [99] D. Martínez, A.M. Campos, F. Pazos, C. Alvarez, M.E. Lanio, F. Casallanovo, S. Schreier, R.K. Salinas, C. Vergara, E. Lissi, Properties of St I and St II, two isotoxins isolated from *Stichodactyla helianthus*: a comparison, *Toxicon* 39 (2001) 1547–1560.
- [100] G.W. Snedecor, W.G. Cochran, *Statistical Methods*, eighth ed., Iowa State University Press, Iowa, 1989.
- [101] J. Tukey, Comparing individual means in the analysis of variance, *Biometrics* 5 (1949) 99–114.

Highlights

- A library of tetrazole-peptidomimetics was obtained by a multicomponent reaction
- Three potent inhibitors of the *E. coli* neutral M1-aminopeptidase were discovered
- High selectivity for the microbial M1-aminopeptidase *versus* the mammalian one
- A non-competitive inhibition mode was found and explained by molecular docking
- *In vitro* antibacterial activity was found for one compound